THE PENNSYLVANIA STATE UNIVERSITY
SCHREYER HONORS COLLEGE

DEPARTMENT OF CHEMICAL ENGINEERING

THE STRUCTURAL EFFECT OF WATER VAPOR ON THERMAL POLING OF SODA LIME GLASS

ERIK SCHNEIDER
FALL 2015

A thesis
submitted in partial fulfillment
of the requirements
for a baccalaureate degree in Chemical Engineering
with honors in Chemical Engineering

Reviewed and approved* by the following:

Seong Kim
Professor of Chemical Engineering
Professor of Materials Science and Engineering
Thesis Supervisor

Michael Janik
Professor of Chemical Engineering
Honors Adviser

* Signatures are on file in the Schreyer Honors College.

ABSTRACT

Thermal poling is an important technique in strengthening and modifying the chemical and mechanical properties of soda-lime glass. This study uses Infrared Spectroscopy (IR) techniques to compare structural changes in the surface of the glass for glasses poled in both a humid environment and an inert environment. The objectives of this thesis were to determine whether and how the presence of water vapor in the environment affect the surface structure of soda-lime glass during poling. Samples were poled in humid (H_2O), inert (N_2), and deuterated water vapor (D_2O) environments for 0, 5, 10, 20, 30, and 40 minutes at 200 C and at an applied voltage of 2 kV. The poled samples were analyzed by SR-IR (specular reflectance) and ATR-IR (attenuated total reflectance) which gave structural information about both the silicon oxygen network and the presence of hydrous species at the surface. Based on the presence of hydrous species in the subsurface region of samples poled in humid environments and the difference in the prevalence of Si-O-Si (bridging oxygen) and $Si\text{-}O^-$(non-bridging oxygen) groups over time between inert and humid poled samples, this thesis confirmed that the environment during poling effects surface structure of the soda-lime glass. The SR-IR and ATR-IR spectra suggested different mechanisms for structural rearrangement and likely different charge carriers in the glass based on environment. The next steps in this research would be to further investigate and confirm how exactly these two mechanisms differ.

TABLE OF CONTENTS

LIST OF FIGURES

LIST OF TABLES

ACKNOWLEDGEMENTS

I would like to thank my thesis supervisor, Dr. Seong Kim, for his guidance in selecting a thesis topic and for granting me the opportunity to conduct research in his group for the past four years. Dr. Kim's passion for investigating the underlying science of engineering problems gave me a standard with which to conduct myself in an engineering laboratory.

I would also like to thank David Marchand and Jiawei Luo for their supervision during my work in Dr. Kim's lab. Without these two graduate students, I would not have been able to succeed in completing the research required for my thesis.

I would like to thank Dr. Janik as well, who initially connected me with the opportunity to work in Dr. Kim's lab. Dr. Janik has been instrumental in helping me get the most of my education at Penn State.

I want to thank my family and friends for their support during my time at Penn State. Their continued support and guidance has helped to make my experience worthwhile.

Chapter 1

Introduction

Soda-lime glass is used in a wide variety of industrial and residential applications such as window panes and glass bottles. It is an ideal material for large scale use because the sodium-containing glass is inexpensive, durable, and recyclable[1]. However, sodium and other modifiers which make up soda-lime glass are disruptive to the internal Si-O-Si structure. To be specific, sodium ions are associated with non-bridging oxygen (NBO) where the silica network is terminated. This structural modification can affect some mechanical properties of the glass compared with pure silica glass. In particular, the structure of the glass at the surface is critical to the mechanical properties of the glass[2,3]. Manipulating the structure at the surface has potential applications in the treatment of inexpensive soda-lime glass in order to improve mechanical properties. Thermal poling is a technique that alters the surface of the glass by applying an electric field across the glass at high temperatures so that sodium ions are forced towards one side of the glass. The thermal poling process changes the chemical structure of the glass that is poled. The primary mechanism for charge movement during thermal poling is the migration of sodium ions from the cathode side of the glass to the anode side as shown in Figure 1.

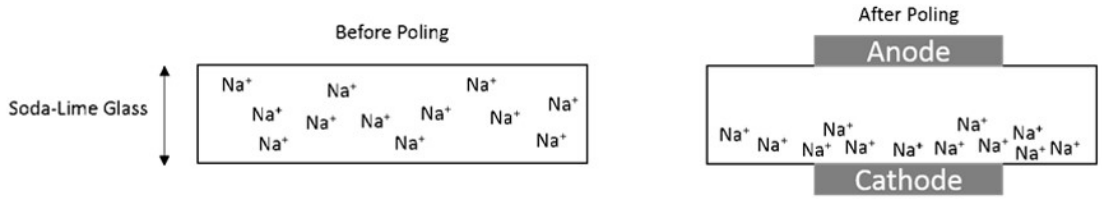

Figure 1: Sodium ion distribution before and after poling.

Once sodium ions leave the subanodic region, charged Si-O$^-$ groups are left behind without positive species to ionically bond to. The structure of this region and the secondary mechanisms for the

movement of charge in the glass have been debated since Carlson proposed oxygen-ion migration towards the anode side of the glass in 1972[4]. Dussauze et al. proposed that the non-bridging Si-O- bond could function as a receiver for protons absorbed from water molecules in the air outside the anode side of the glass towards the cathode side[5]. The possibility that water vapor from the air could be absorbed into the surface of the glass and subsequently transferred to binding sites in the silicon oxygen network in various forms is important to investigate. In order to determine the effect of water vapor on the mechanism of thermal poling and the resulting glass structure, poling in H_2O vapor and D_2O vapor rich environments was compared to poling in an inert (N_2) environment. To compare structures, specular reflectance infrared spectroscopy (SR-IR) and attenuated total reflectance infrared spectroscopy (ATR-IR) were utilized. A brief discussion on the structure of soda-lime glass, the thermal poling process, the use of ATR-IR and SR-IR for analysis of surface structure, and the current proposed secondary ion movement mechanisms will follow.

Structure of Soda-Lime Glass

Understanding the structure of soda-lime glass prior to poling is critical to understanding the structural changes that occur during the poling process. A combination of Si- O-Si bridging bonds and sodium and calcium ions bonded to $Si\text{-}O^-$ non-bridging oxygens create a random Si-O network throughout the bulk of the glass[6,7]. Non-bridging oxygen atoms are attached to one silicon atom but are not held in place by a second silicon atom, and thus are negatively charged and attracted to cations in the network. Figure 2 shows a basic soda-lime glass structure.

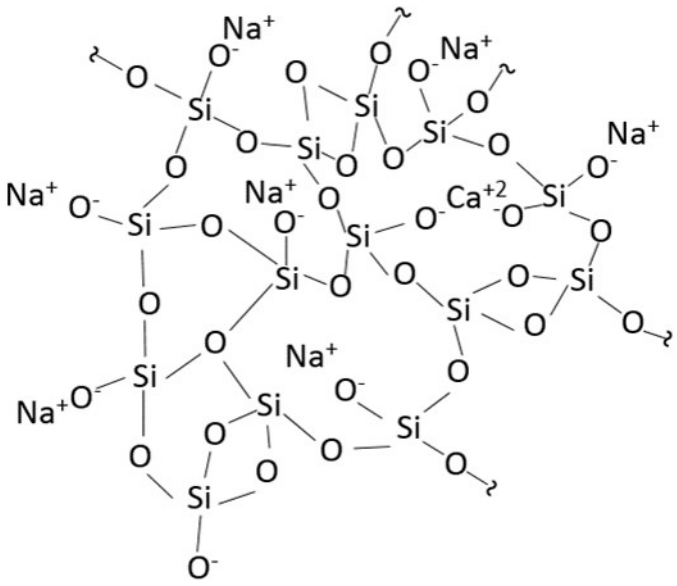

Figure 2: Example chemical structure of soda-lime glass.

The movement of positively charged sodium ions to the cathode side during poling is also a generally agreed upon phenomenon and is well documented in the literature[4,5,8]. The movement of sodium ions through the network of oxygen and silicon during poling is caused by the very strong external electric field. The sodium ions are initially held in place by their electrostatic attraction to the negatively charged non-bridging oxygens, but easily move through the glass when a potential difference is applied. The movement of the sodium ions out of the silicon-oxygen network leads to voids where negative charges exist transiently. As mentioned previously, multiple theories predict what happens to these negative charges during and after the poling process.

One important hypothesis is that chemical species like water molecules can be absorbed into the subsurface region of the glass structure from the environment and subsequently transferred to the voids left by the sodium ions. The water can also form hydronium ions which can associate with NBO groups.

Wear behavior of unpoled soda lime glass has been found to be dependent on the humidity of the environment, suggesting that the surface structure of the glass and its interaction with water are important

determinants of mechanical responses[9-11]. Furthermore, hydronium ions and hydrous species at the surface of soda-lime glass have been found to improve wear resistance[10-12]. For these reasons, the effect of a humid environment during thermal poling will be investigated. In order to determine the structural effect of thermal poling, a brief overview of thermal poling and a discussion of SR-IR and ATR-IR techniques will follow.

Thermal Poling Process

During the thermal poling process, a potential difference is applied across the glass surface at elevated temperatures. At high temperatures, sodium ions can escape the silicon-oxygen network and, because of the potential difference, the ions can electrostatically move toward the cathode in the poling process. Additional charge moves through the glass, and the charge movement creates a measurable current. The relationship between current and charge is shown in Eq. 1.

$$Q = \int I dt \tag{1}$$

By measuring the current during the thermal poling treatment, the approximate amount of charge moving through the glass over a given period of time can be determined. Alley et al. found that the current measured during the thermal poling process cannot be explained simply by the movement of sodium ions, but that multiple ionic species must move through the glass[13]. Although in-depth analysis of the current profiles was not used to analyze poling results in this thesis, qualitative analysis of current versus time plots was used to initially analyze experimental results. Figure 3 shows an example current versus time plot for a soda-lime sample that was poled for 40 minutes in air.

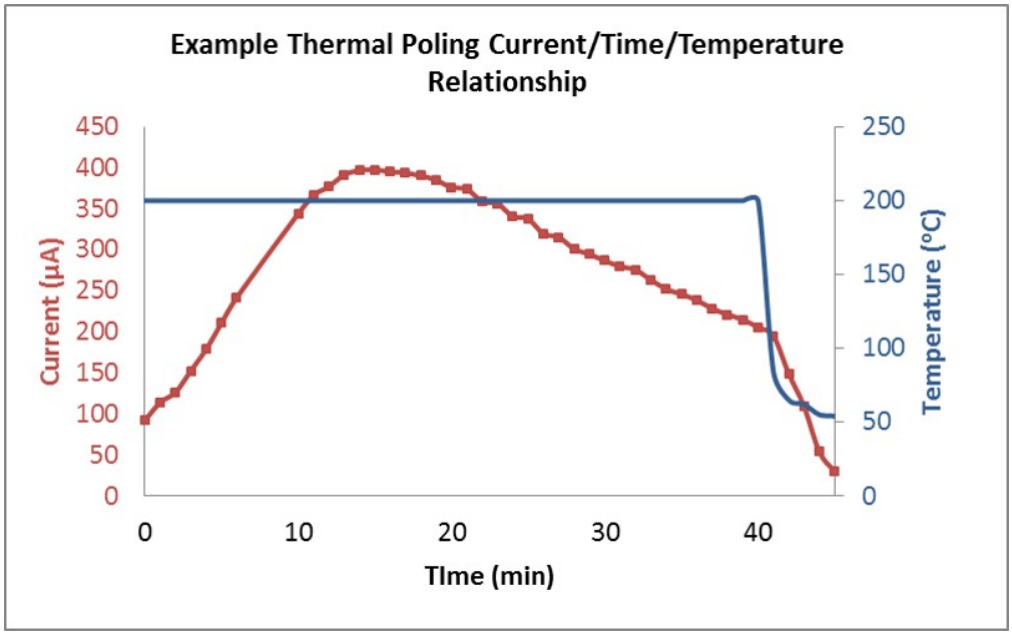

Figure 3: Example current and temperature versus time plot for thermal poling procedure.

As can be seen in the figure, the current begins to decrease well before the temperature is decreased by the operator. By the end of the 40 minutes, the number of ions moving and thus the effect of the potential difference on the glass, has dropped considerably. This suggests that the overall impedance of the glass changes during the poling process. At the beginning, sodium is rich near the electrode and the overall impedance of the glass is close to the impedance of pristine soda lime glass. As poling proceeds, sodium ions are transported to the cathode side, which results in a layer with fewer sodium ions. Thus the overall impedance become the combination of the sodium depleted layer and the bulk of the regular soda lime glass, the absolute values of which increase over time and contribute to the decrease of the current.

Use of SR-IR and ATR-IR for the analysis of glass surfaces

IR is the method of choice for investigating the effects of humid environments on thermal poling because IR can detect bridging and non-bridging oxygen groups in addition to molecular water and hydrous

species in the glass structure[14-16]. There are three methods typically used in IR analysis: transmission, specular reflectance, and attenuated total reflectance. A picture of the how the two surface-sensitive techniques, SR-IR and ATR-IR, work is shown in Figure 4.

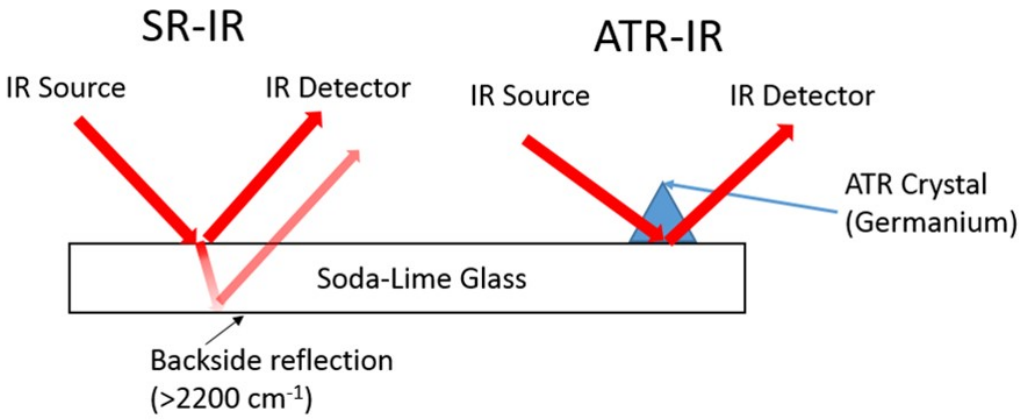

Figure 4: Specular reflection (SR), and attenuated total reflection (ATR) IR techniques.

ATR-IR and SR-IR are both surface-sensitive and thus useful to the present analysis; however, in SR-IR there is the possibility of a contribution from backside reflection as shown by the dull red arrows in Fig. 4. In SR-IR, a positive signal is generated when the frequency of the incoming IR source matches the absorption of a species in the glass. This match in frequency intensifies the reflected IR beam which is why positive peaks in SR-IR are an indication of the presence of specific vibrational modes of chemical bonds[14]. ATR-IR uses a germanium crystal in close physical contact with the glass sample. Since germanium has a higher refractive index than the glass sample, the total reflection will happen at the Ge-glass interface when the incident angle of the IR beam is at 45 degrees[14,17,18]. Therefore, only an evanescent wave can propagate to the glass and be absorbed by the glass. The penetration depth of the evanescent wave in the case of this study is between 0.4 to 1 microns[14]. ATR-IR is thus very useful for observing the changes in the surface region of the glass without interference from the other side or from the bulk of the glass as is the case with SR-IR. One disadvantage of ATR-IR is the technique is not sensitive to small differences in Si-O-Si bridging vibrations which are a key part of the analysis of

thermal poling[14]. Because of higher penetration depth at lower wavenumbers, backside reflection in SR-IR only needs to be taken into account at wavenumbers above ≈2200 cm^{-1}. Because Si-O-Si asymmetric vibrations exhibit a peak around 1100 cm^{-1} and $Si-O^-$ structures exhibit a peak at 940 cm^{-1} , SR-IR can be used to analyze these structures; ATR-IR can be used to analyze the presence of water and other hydrous species at the surface which show up at wavenumbers above 2200 cm^{-1}. Amma et al. calculated penetration depth in SR-IR as a function of wavenumber for soda-lime glass as shown in Figure 5.

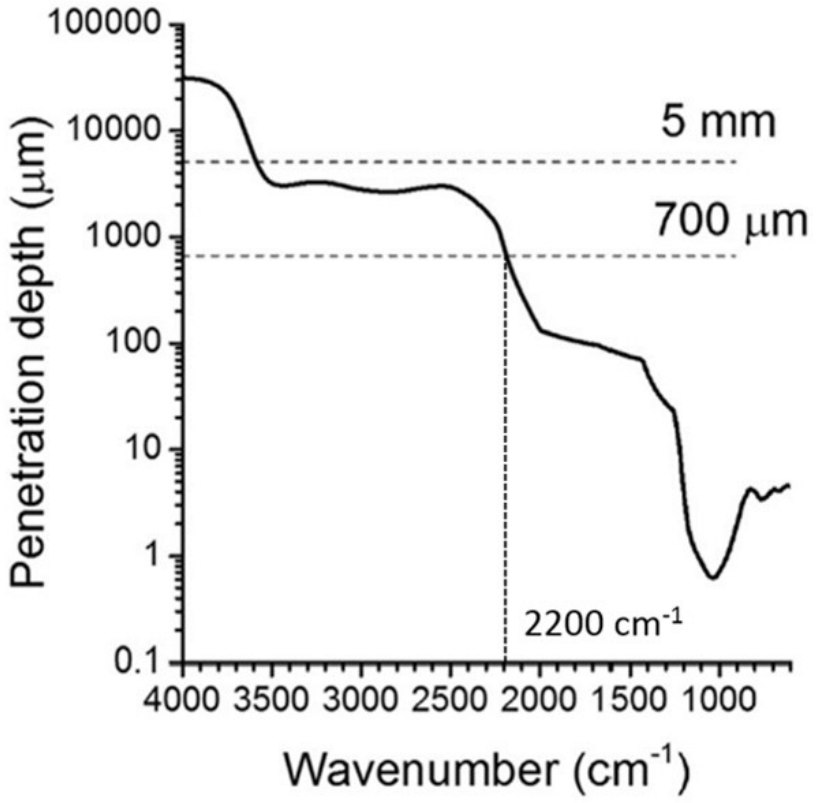

Figure 5: Penetration depth of SR-IR beams in soda-lime glass. Image Credit: Amma et al[14].

In the analysis of soda-lime glass, there are several regions and peaks of signature importance when evaluating the presence of hydrous species and when evaluating the silicon-oxygen structure. In the backside reflection region, negative peaks at 2800 cm^{-1} and 3400 cm^{-1} indicate the presence of hydrous species in the bulk, however because of backside reflection these peaks are not useful since peaks cannot

be distinguished as originating from the cathode surface or the anode surface[14]. 1050 cm^{-1} is the asymmetric stretching vibrational peak of Si-O-Si groups and the shift of this group provides important structural information[19,20]. If this peak blue-shifts it becomes more like pure silica which, as mentioned previously, has a peak at 1122 cm^{-1}. Another peak of interest in the SR-IR spectra is at 940 cm^{-1} which is the stretching vibration of the Si-O bond in non-bridging groups and so can be attributed to either $Si\text{-}O^-$ (non-bridging) or Si-OH groups[10,14]. In the ATR spectra, the OH stretching vibration creates a broad peak between about 3650-2500 cm^{-1} because of the hydrogen bonds associated with the presence of various Si-OH and H_2O species[14]. In addition, the sharp peak at 1650 cm^{-1} indicates the presence of molecular water in the glass network. Importantly, when D_2O replaces H_2O, the Si-OD and D_2O peaks red-shift, which will be important in distinguishing whether water was introduced from the environment during poling or was naturally absorbed into the surface[14].

Theories of Ion Movement in Thermal Poling

Although thermal poling in humid environments cannot provide final, conclusive evidence for the acceptance of one of the many proposed mechanisms for ion movement during thermal poling, the role of water in these mechanisms can be analyzed. In that interest, a brief overview of some of the main theories for the mechanism of thermal poling is provided.

Carlson et al. suggest that non-bridging oxygen ions move through the glass against the flow of sodium ions, towards the anode side[4]. Carlson's findings have been backed up by further studies on mechanisms in play during thermal poling[5,21,22]. Carlson et al. claim that in order for oxygen ions to be mobile they must break their bond with the silicon atom they are initially attached to[4]. This phenomenon is possible considering the high energy applied to the glass and due to the weak nature of the Si-O- non-bridging bond. Researchers agree that if oxygen ion movement occurs it must be due to the breaking of the non-bridged oxygen-silicon bond. Kreiger and Lanford present another possibility: the unbridged

oxygen ions could just as easily act as electron carriers[8]**.** The electrons would create the same effect of negative charge moving towards the anode side of the glass as oxygen ions, but would not require the breaking of a silicon-oxygen bond in the process. Dussauze et al. propose that the non-bridging Si-O- bond could function as a receiver for protons flowing from water molecules in the air outside the anode side of the glass towards the cathode side[5].

Lepienski et al. conclude that, when a blocking electrode is used, oxygen ion movement explains thermal poling but that, when a blocking electrode is not used, proton movement into the glass from water molecules in the air is the *dominant* mechanism for charge movement[21]. Non-blocking electrodes allow the environment to contact the glass surface while blocking electrodes do not. While many mechanisms have been proposed and supported with experimental evidence, none have been accepted by the entire poling community.

While many theories do not involve hydrogen or hydrous species, there is significant evidence to suggest that they at least play a role in some poling configurations. Carlson found that, in poling of soda-lime glasses, protons moved into the sodium-depleted region of the glass and that the protons were absorbed from the air[23]. Carlson also concluded that the protons bind to the Si-O network in multiple ways in this region[23]. Ernsberger argued that when water is absorbed by the subanodic region of the glass it is oxygenated[24]. In an experiment not involving thermal poling, Lanford et al. proposed that H_3O^+ was the main group that replaces sodium in sodium depleted regions of soda-lime glass[25].

The current thesis seeks to investigate specifically the role of a humid environment during thermal poling on the surface structure of the poled glass. Although similar studies have been completed to investigate both the structure of glass after poling and how hydrogen species interact with the glass structure, the current thesis looks exclusively at structure using SR-IR and ATR-IR techniques which uniquely characterize the species present.

Chapter 2

Experimental Methods

Sample Preparation

Asahi Glass Co. Ltd. in Japan supplied 0.7 mm thick soda lime float glass samples for use in the thermal poling experiments. The flat glass surface was produced by floating the glass melt on a tin bed, which results in tin residuals on one side of the glass which is appropriately called the “tin side”. The other side of the glass is called the “air side”. To rule out complications for the surface analysis, all the analyses are reported on the air side of the glass. While this glass has similar composition to most soda-lime glasses, the chemical composition was determined by Amma et al. in a previous study by x-ray fluorescence. The results of the XRF study are displayed in Table 1, below.

Table 1: Soda-lime glass composition from XRF study. Data Credit: Amma et al.[14]

Compound	**SiO_2**	**Al_2O_3**	**MgO**	**CaO**	**Na_2O**	**K_2O**	**Fe_2O_3**
Mol%	70.8	1.0	6.2	9.1	12.5	0.4	0.04

Prior to poling, samples were cut into rectangles approximately 3.5” x 1.5” and subsequently washed with DI water and exposed to an ozone environment for 10 minutes. The cathode in the thermal poling apparatus was always placed on the air side of the glass.

Thermal Poling Conditions

A diagram of the thermal poling apparatus used is shown below in Figure 6.

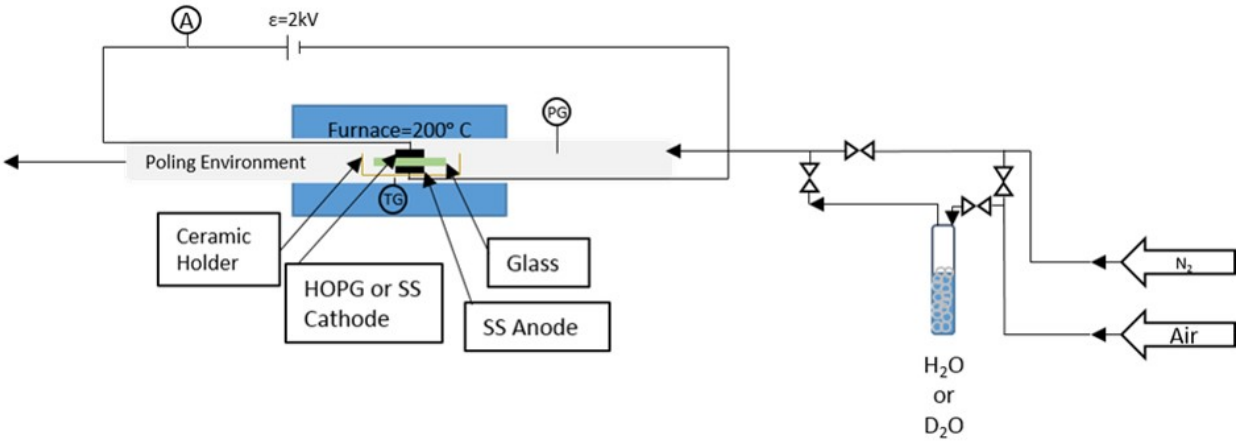

Figure 6: Thermal Poling apparatus diagram.

Soda-lime glass was sandwiched between a non-blocking stainless steel anode and a non-blocking stainless steel or HOPG cathode. The poling area was determined by the size of the cathode and measured approximately 0.75" x 0.75". Once loaded, the sample was allowed to heat to a temperature of 200° C in the furnace and during this time the environmental conditions for the poling process were introduced. For a nitrogen environment, N_2 gas with a flow rate of 3 L/min was introduced to the sealed poling environment. Compressed air was introduced to the poling environment the same way. The nitrogen gas, water vapor, and D_2O vapor were all introduced at room temperature to the heated glass samples.

The water vapor in air introduced into the poling chamber could potentially wick a small amount of heat away from the surface of the glass. However, because of the low heat transfer coefficients of gases, this effect is negligible. Using Newton's law of heating and heat transfer coefficients calculated for forced convection over a flat plate, the heat transfer from the glass surface can be estimated for both nitrogen gas and humid air. Equation 2 below shows Newton's law of cooling.

$$q = hA\left(T_{surface} - T_{fluid}\right) \quad (2)$$

Where $T_{surface}$ is equal to 200 C since the oven maintains the surface at this temperature, T_{fluid} is at room temperature and equal to approximately 20 C (which is a worst case assumption, in reality the fluid temperature is higher than room temperature because it has been heated by the furnace), A is the area of the glass sample which is approximately 0.0034 m^2. The reason this effect is not important is the very small difference in the heat transfer coefficients for nitrogen and humid air, even when the actual temperature of the gas is not used and when the temperature control of the furnace is not taken into account. For nitrogen the heat transfer coefficient was calculated to be 1.77 W/m^2K and for humid air the heat transfer coefficient was 1.71 W/m^2K. Carrying through the math, the amount of heat lost to the flowing air was 1.6 J/s and 1.7 J/s lost to flowing N_2. So, not only is the amount of heat transferred from the glass surface very small in magnitude, both samples were exposed to about the same effect and thus this heat transfer could not influence the results of the experiments significantly.

To create a humid environment, compressed air with a flow rate of approximately 3 L/min was bubbled in either H_2O or D_2O liquid, creating a saturated H_2O vapor or D_2O vapor. A picture of the bubbling apparatus used is shown in Figure 7.

Figure 7: Apparatus for introducing humid environment.

Once temperatures stabilized at 200° C, samples were poled for 5, 10, 15, 20, 30, or 40 minutes. Each sample was exposed to one type of environment during the whole poling process. At the end of the allotted time, the furnace was turned off and the whole system was allowed to cool to room temperature at 2 kV, so that ions would not relax back to original locations when the potential difference was taken away. Once samples cooled to room temperature, the potential difference was turned off so that sodium and other ions that had moved would no longer have the thermal energy required to move back to their original location[26]. The poling was carried out at ambient pressures. During the poling process, current and temperature were recorded every minute and plotted against time. An example of these measurements was explained in the introduction in Figure 3.

SR-IR and ATR-IR Measurements

ATR-IR measurements were taken using a Bruker Hyperion μ-FT-IR system with an attached infrared microscope objective lens from Bruker Optics Inc. capable of 15x magnification. A Germanium ATR crystal was pushed onto the glass surface at 600 N over a 1 cm^2 area. SR-IR measurements were taken at a 40° incidence angle with a Thermo-Nicholet 670 FT-IR system. SR-IR spectra were taken between 4000-500 cm^{-1} and samples were cleaned with DI water and ozone prior to measurement. ATR-IR measurements were taken between 4000-1400 cm^{-1}. Backgrounds for the SR-IR spectra were obtained using a gold mirror and air was used as the ATR-IR background.

Based on Figure 5 in the introduction the penetration depth of the SR-IR technique changes with the frequency of the IR beam. The penetration depth ranges from only about 1 μm at 1000 cm^{-1} to 700 μm at 2200 cm^{-1}. So, the SR-IR measurements were taken on the glass samples with the idea that depending on the frequency of the absorption band, the reflectance profile would have more surface information or more bulk information.

The penetration depth of the ATR-IR technique is dependent on the type of ATR crystal, angle of the IR beam and the sample[14,27]. The range of possible penetration depths is much smaller than the range for SR-IR and is usually between 0.5 and 3 microns[27]. The low ATR penetration depth is the reason it is used to determine the surface structure of the glass above 2200 cm^{-1} where backside reflection becomes a significant problem for SR-IR. SR-IR does give more reliable information about Si-O-Si structures than ATR-IR because ATR-IR, in that region of the Si-O-Si absorption bands, has too complex of a refractive pattern to yield conclusive results[14]. Thus, spectra from both SR-IR and ATR-IR were collected and are analyzed in the following section.

Chapter 3

Results and Discussion

Current Profile

Qualitatively, the current versus time plots for poling in different environments can be compared to establish differences between magnitudes of charge movement between the samples. Figure 8 shows current versus time plots for poling of nitrogen flow and water vapor flow of 40 minute poling time samples and the calculated total charge versus time for each sample.

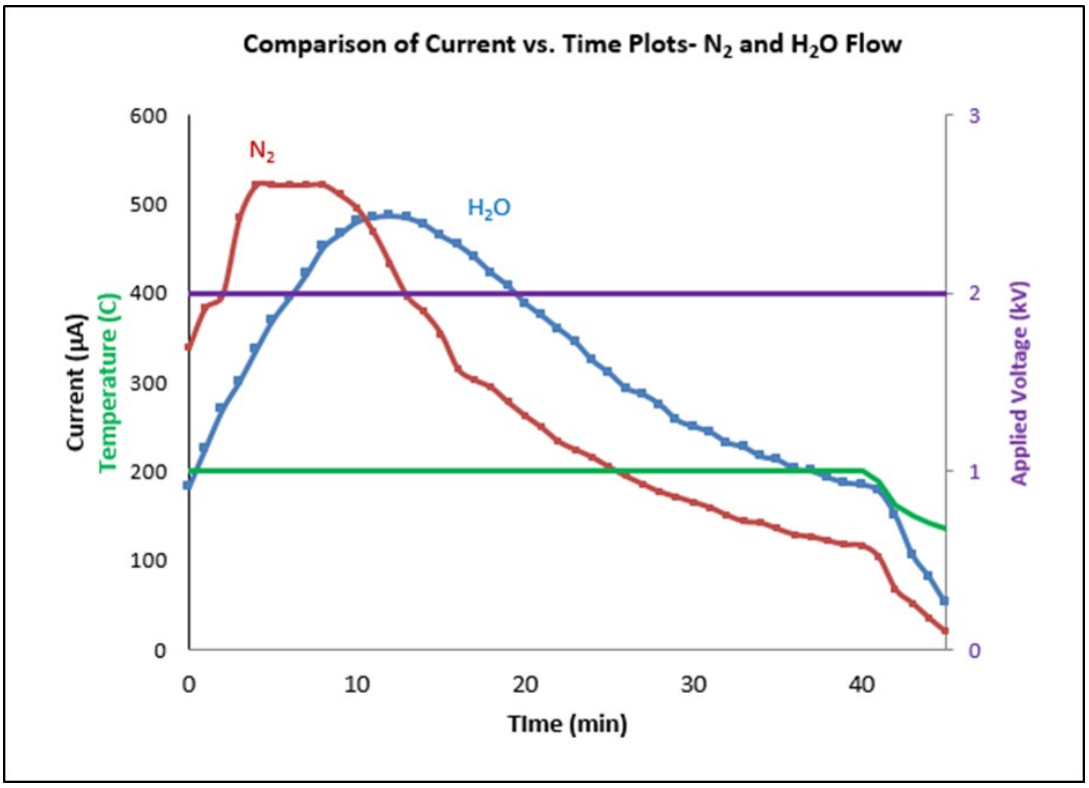

Figure 8: Current and total charge versus time comparison for N_2 and H_2O samples

Figure 8 shows that the current value for the H_2O flow sample does not reach the maximum of the N_2 sample. However, this "maximum" based on the current versus time plots is highly variable and is not consistent across all poling experiments. The magnitude the current reaches is inconclusive with respect

to the structural rearrangement. The consistent result of the poling experiments—displayed in Fig. 8—is that the current for the samples poled in more humid environments drops off less quickly than samples poled in inert environments. In the H_2O flow samples, the sodium ions move through the glass and create current just like in the nitrogen poled samples, but once the charge carriers are done moving, hydrogen species can move through the glass from the environment and continue to generate a current. In the nitrogen samples, which drop off quicker in current, there are less charge carriers to continue to generate a strong current. For samples poled for different lengths of time, the total charge passing through the glass during poling can be compared for nitrogen and humid poled samples. Figure 9 shows the comparison of total charge versus poling time for both the samples poled in H_2O vapor and the samples poled in N_2 samples.

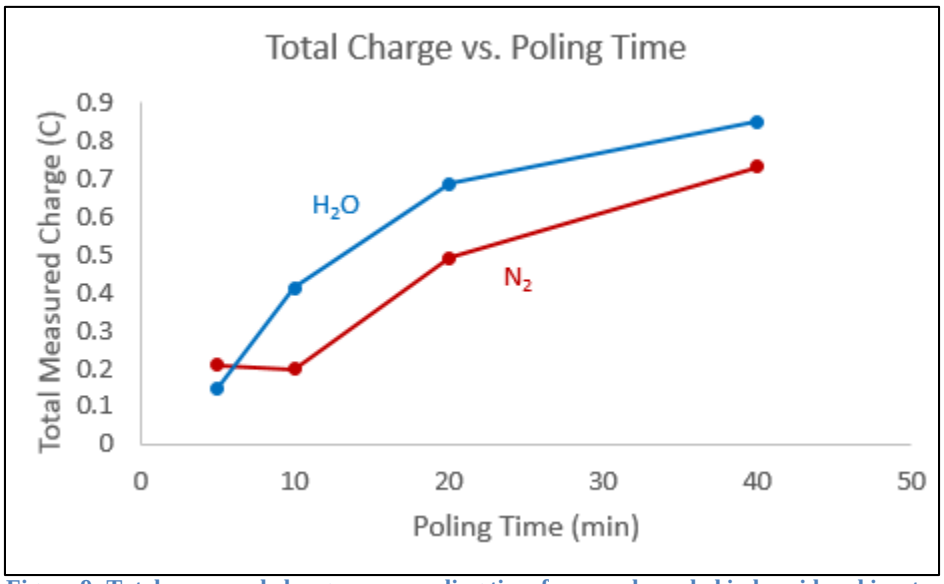

Figure 9: Total measured charge versus poling time for samples poled in humid and inert environments.

The Nitrogen total charge value for 10 minutes poling time does not fit the trend and expected result for total measured charge; this experiment should be repeated to see whether or not the total charge for 10 minutes does fall between the total measured charge for 5 and 20 minutes of poling. Even given the out of place data point, the trend for both the samples poled in water and nitrogen seems to be logarithmic and reaches some maximum total charge movement value. So, as has been shown, poling cannot continue to

work after a given point most likely because of a lack of mobile charge carriers remaining in the glass. The samples poled in water do seem to have a higher maximum charge movement, most likely because of the extra charge carriers present in the atmosphere. By integrating the current over time as shown in Equation 1, the depth of the sodium depleted layer can be calculated by Equation 3 below[22]:

$$l_d = \frac{\int_0^t I(t)dt}{AeN_{Na}} \tag{3}$$

where I(t) is the current, A is the surface area poled, e is the elementary charge, and N_{Na} is the sodium concentration per unit volume in the soda lime glass. In this case, the numerator will depend on the particular poling experiment, A is 0.5" x 0.5" which equals 1.61 cm^2, e is 1.602 x 10^{-19} C, and N_{Na} can be calculated from the glass's density and composition and is found to be approximately 6.3 x 10^{21} Na atoms/cm^3. Assuming Na is the only charge carrier (which is not necessarily a valid assumption) the sodium depletion layer for the 40 minute nitrogen poled sample is approximately 4.5 μm while the sodium depletion layer in the 40 minute water poled sample is approximately 5.2 μm. Most likely, this difference in calculated depletion layer is a result of the fact that a secondary charge carrier takes over once sodium has been depleted in the top 4.5 μm of the subanodic region. IR spectra of the poled samples will be used to show that hydrogen species move into the glass. If any conclusions are to be drawn from this observation, future work will have to focus more in depth on current profiles in different environments.

SR-IR Results

The specular reflectance IR results for the different poled samples give information on the structural changes in the glass both at the surface and in the bulk of the sample. As shown in Figure 5, the SR-IR technique shows surface characteristics below about 2200 cm^{-1}, specifically the Si-O-Si structure, and above 2200 cm^{-1} SR-IR includes backside reflection and will be shown to be inconclusive for this

thesis. Figure 10 below shows SR-IR spectra of the anode side of the glass, poled in water and nitrogen environments, as well as a "no poling sample" showing an area of glass not poled at all. (In this case the "no poling" IR data was taken from the glass poled in the N_2 environment; however, this particular area was not subjected to any poling.)

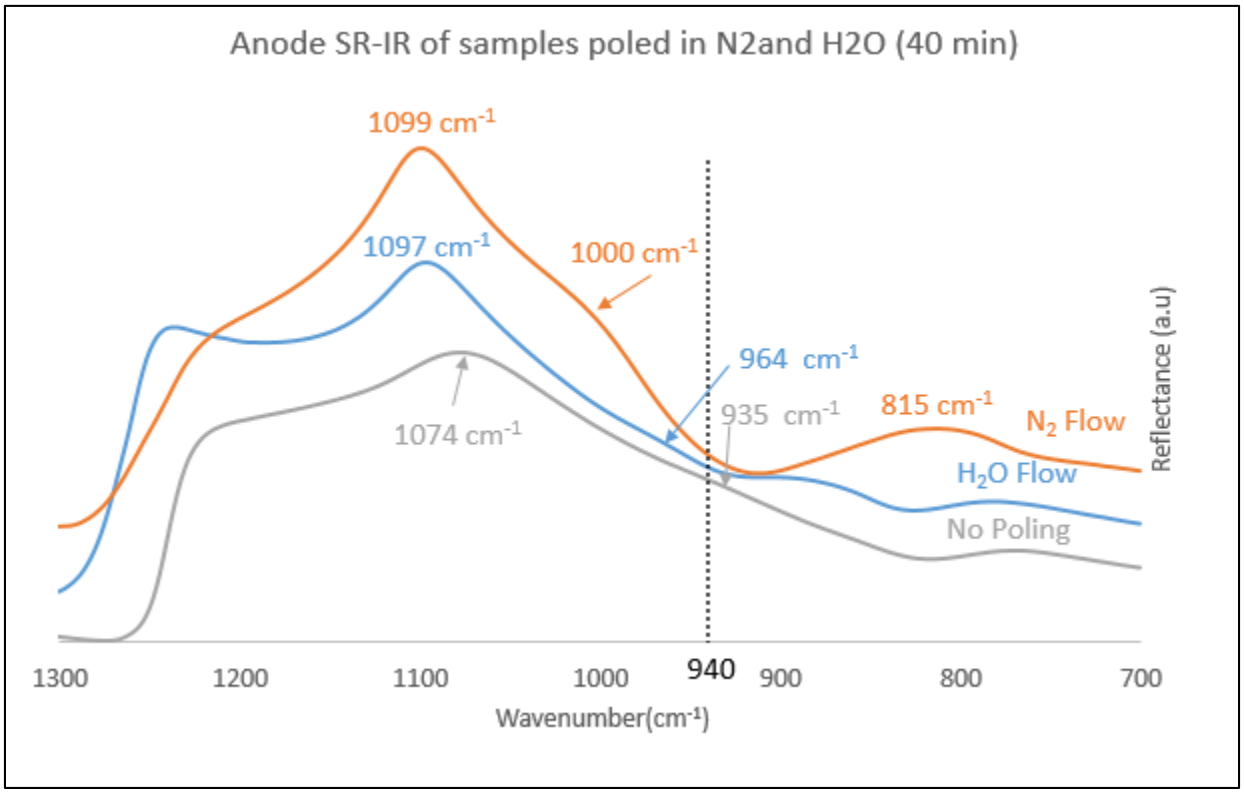

Figure 10: SR-IR spectra of anode side of poled glasses from 700-1300 cm-1.

In Figure 10, the blue-shift of the Si-O-Si peak from 1074 cm^{-1} in unpoled glass to 1097 cm^{-1} in glass poled in a humid environment is the most noticeable result. Interestingly, both the sample poled in a humid environment and the sample poled in a nitrogen environment have peaks at approximately 1098 cm^{-1}. Since pure SiO_2 (quartz) has the Si-O-Si bridging peak at 1122 cm^{-1}, this blue shift is the expected result: as samples are poled and sodium ions vacate the anode side of the glass, a more Si-O-Si rich network is formed. The difference in poling environments clearly does not create a significant difference in the Si-O-Si bridging structure at the anode side of the glass after 40 minutes of poling. The $Si\text{-}O^-$ non-bridging vibration at around 940 cm^{-1} is a peak of interest in this case. Unlike the Si-O-Si bridging peak,

the variation of the non-bridging peak is barely noticeable. For the pristine sample, the peak is around 935 cm^{-1}, which is close to the expected peak, and very small which most likely indicates small amounts of Si-O^- ionically bonded to Na^+. Once the poling occurs, however, the peak drastically blue-shifts and becomes slightly more intense in humid conditions after 40 minutes of poling. The peak blue-shifts even further, to 1000 cm^{-1}, after poling in the nitrogen environment. The blue-shift in both the poled samples indicate that once sodium leaves the subanodic region, the Si-O^- groups rearrange and either form Si-O-Si structures or are protonated and form Si-OH structures (which form more hydrogen bonds and thus could cause a blue-shift). The intensity increase indicates an increase in Si-O^- groups, which is highly unlikely since the conjugate ion, Na^+ is depleted in the subanodic region. An increase in prevalence of Si-OH groups must be responsible for this peak shift and increase in intensity[10]. The N_2 sample could have blue-shifted more than the H_2O sample because Si-O^- conversion to Si-O-Si groups in the N_2 was more prevalent than conversion to Si-OH groups. In addition, the broad peak appearing at approximately 820 cm^{-1} only in the N_2 poled spectrum is most likely the result of the symmetric vibration of Si-O-Si groups. This peak appears in amorphous silicon oxygen structures and is a result of the bridging oxygen network created in the subanodic surface region for samples poled in nitrogen[28]. The appearance of this peak in only the nitrogen poled sample gives further evidence that rearrangement to bridging oxygen groups occurs more when poling in a nitrogen environment because of a lack of stabilization of NBO groups by hydrous species.

To further investigate how the Si-O-Si bridging structure changes during poling, SR-IR spectra of samples poled for various durations (0, 5, 10,20,30,40 mins) are compared; the anode side of both the samples poled in water vapor and the samples poled in nitrogen are displayed. The anode SR-IR spectra for the samples poled in the humid environment are shown below in Figure 11.

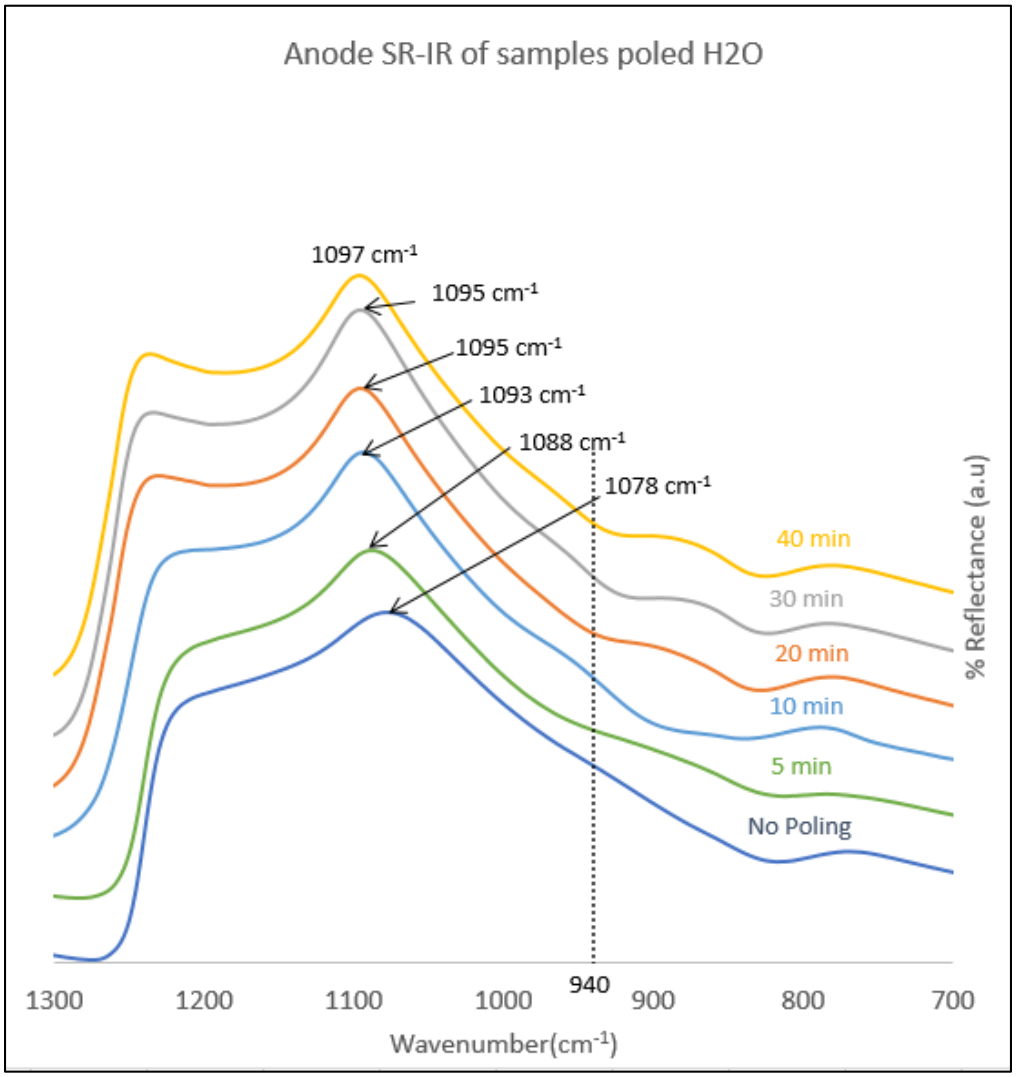

Figure 11: Anode SR-IR spectra of samples poled in a humid environment for 0, 5, 10, 20, 30, and 40 minutes.

Figure 11 shows a blue shift towards a more pure Si-O-Si bridging network structure. With no poling, the air side of the soda lime glass has a Si-O-Si asymmetric vibrational peak at 1078 cm^{-1}. As poling time increases, the peak blue shifts gradually until it eventually hits 1097 cm^{-1} after 40 minutes of poling. So, as time increases the surface depleted in sodium ions is creating a structure with more and more Si-O-Si bridging character. Also, the non-bridging oxygen peak at 940 cm^{-1}, which while hard to notice, does blue-shift with time in this case. For the no poling sample, the peak is at 935 cm^{-1} but for the 10, 20, and 40 minute samples the peak shifts over to about 960 cm^{-1}. The peak is not noticeable for the 5 minute and

30 minute samples which could be due to a variety of reasons, but is most likely a result of the very small magnitude of the peak and the inconsistent surface structure of the glass. This blue-shift again most likely means that more Si-OH groups are replacing previously $Si\text{-}O^-$ groups in the glass network. The activation barrier for formation of Si-OH groups from $Si\text{-}O^-$ groups is less than the barrier to form a new Si-O-Si group and thus in the presence of hydrous species, Si-OH groups are formed faster. In conjunction with the shift of the Si-O-Si peak, the shift in the 940 cm^{-1} peak most likely represents a shift $Si\text{-}O^-$ groups to Si-OH groups at the subanodic surface[10]. Thus, the humid environment is assisting in the rearrangement of the glass structure, *even after the sodium has stopped moving*. The water moving into the structure is most likely responsible for the gradual, but continuous blue-shift of the Si-O-Si peak and changing network of Si-O-Si bonds. Figure 12 shows the spectra from the anode side of the samples poled in nitrogen over time.

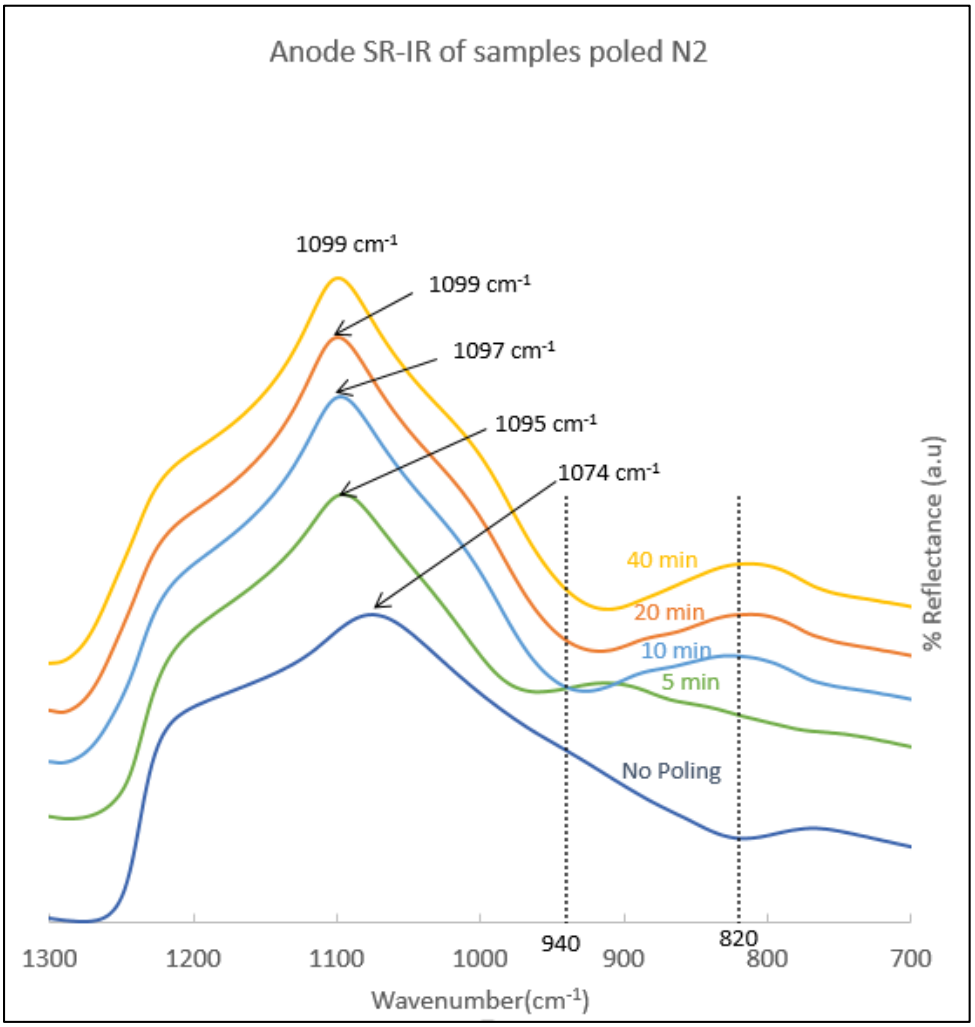

Figure 12: Anode SR-IR of samples poled in a nitrogen environment for 0, 5, 10, 20, and 40 minutes. Data Credit: Jiawei Luo.

An interesting phenomenon occurs over time for the N_2 environment samples. After just 5 minutes of poling, the Si-O-Si asymmetric vibrational peak blue-shifts to 1095 cm^{-1} which is very close to the full shift that occurs after 40 minutes. Most of the change in Si-O-Si bridging structure on the anode side happens in the first 5 minutes of poling. So, although the final Si-O-Si peak is very similar to the peak observed in the samples poled in a humid environment, the way the structure changes throughout poling is different. The $Si\text{-}O^-$ peak position is blue shifted significantly from the no poling peak at about 940 cm^{-1}. The shift to approximately 1000 cm^{-1} is noticeable and essentially stays constant for the 10, 20, and 40 minute spectra. Again, it seems as if for the nitrogen sample, the $Si\text{-}O^-$ peak suddenly shifts because

most of the $Si\text{-}O^-$ converts to Si-O-Si relatively quickly. In this case, there are very few available protons and hydrous species to bind to the empty $Si\text{-}O^-$ groups, so they form a bridging bond more quickly than when water in the environment is present. Both trends support the idea that in nitrogen poling the environment makes the structure become more Si-O-Si like more quickly. In addition, after just 10 minutes of poling a broad peak at about 820 cm^{-1} appears, which is the symmetric stretching peak of bridging oxygen bonds. This peak again shows that the nitrogen poled samples create a surface structure more prevalent in Si-O-Si groups than samples poled in a humid environment. Further experiments are required to confirm that the 820 cm^{-1} peak in these spectra is a result of the bridging oxygen stretching vibration.

From the spectra plots over time for the two environments, two different structural modification mechanisms are present during the poling: the NBO is restructured to form Si-O-Si and NBO is associated with protons or hydronium ions as sodium is removed. It is possible that during the nitrogen poling, the sodium ions quickly move out of the anode side and because of an absence of any other positive charge carrier, NBO groups quickly convert to Si-O-Si groups and stay that way throughout the poling. Therefore, the restructuring of NBO dominates in this process. In humid environments, hydronium ions and molecular water may move into the structure, initially stabilizing the NBO groups in the sodium depleted region and creating Si-OH groups. However, as time goes on, and charge moves slower and slower, the $Si\text{-}O^-$ and Si-OH groups slowly convert to Si-O-Si groups. The two mechanisms are thus competing during the poling process. The spectra on the cathode side of the glass as a function of time in both poling environments are shown below in Figures 13 and 14.

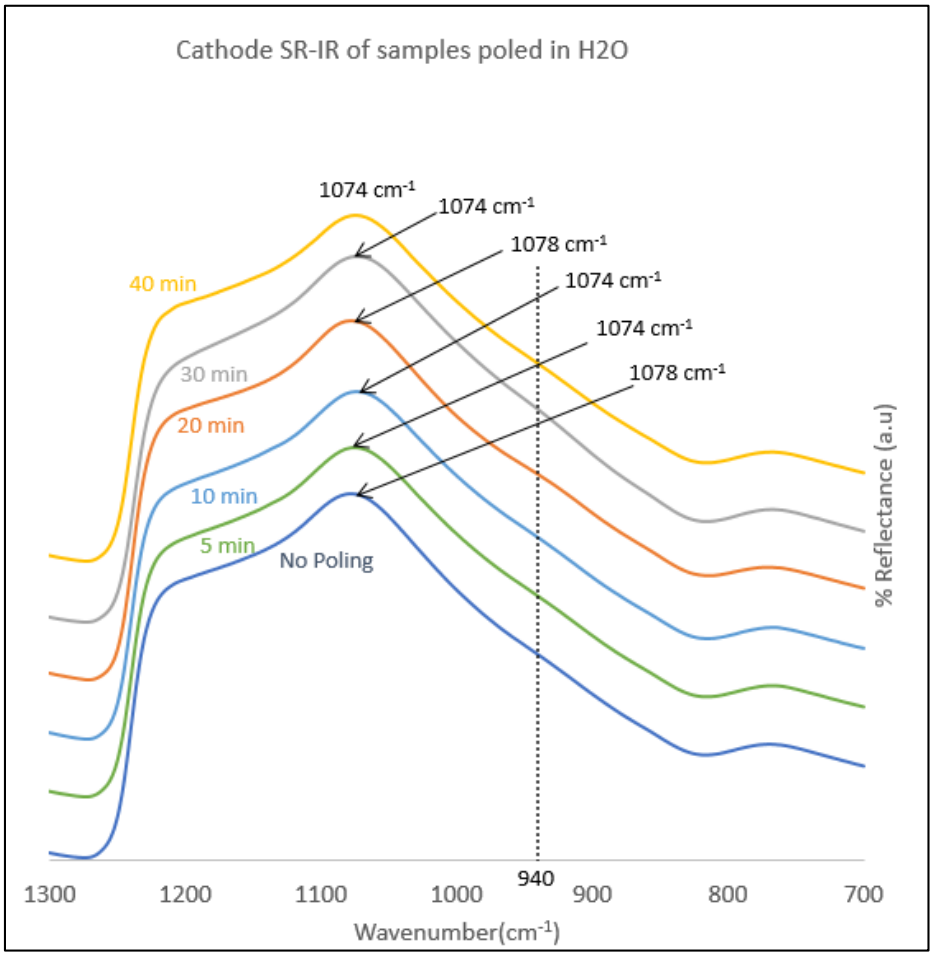

Figure 13: SR-IR spectra of cathode side of glass for different poling times.

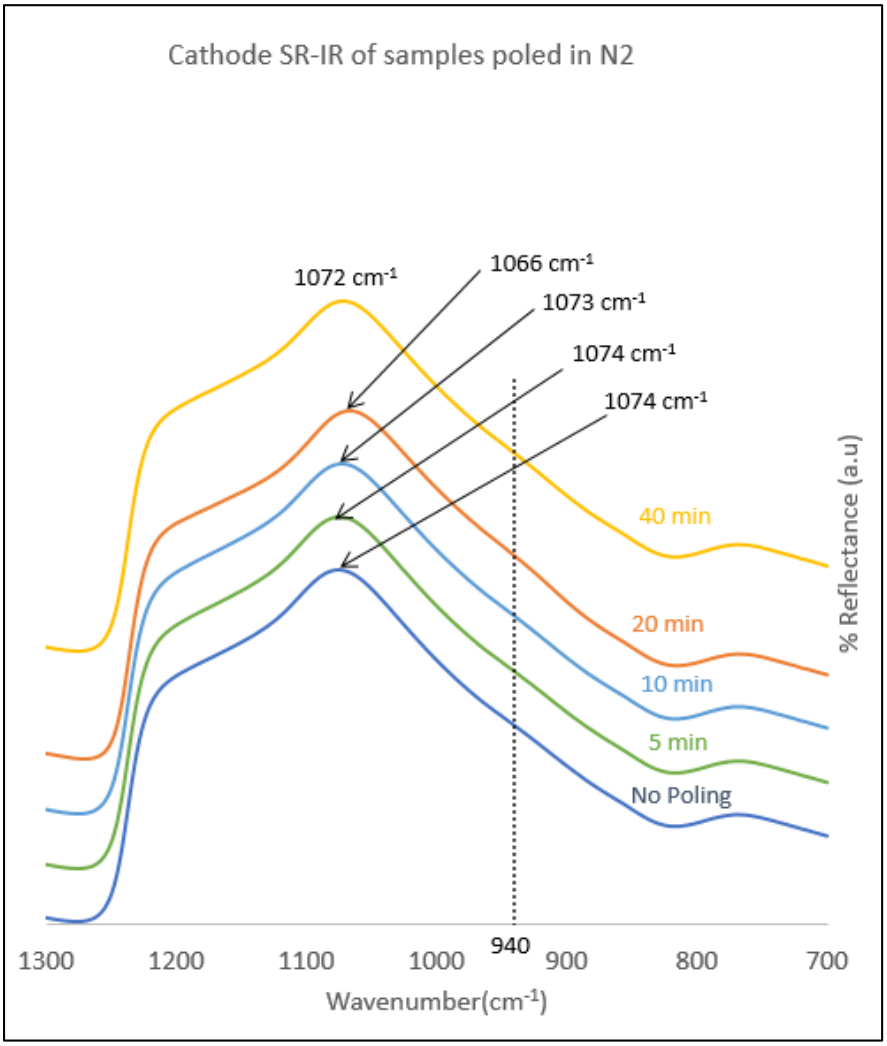

Figure 14: SR-IR spectra of samples poled in nitrogen environment for different poling times. Data Credit: Jiawei Luo.

Unlike the anode side of the glass, there is no significant observable shift in the Si-O-Si vibration peak on the cathode's spectra for either the samples poled in a humid environment or the samples poled in the nitrogen environment. Since the cathode side receives sodium ions, a change in the Si-O-Si bridging structure is not expected: no sodium ions leave the cathode side so there is no room for more Si-O-Si structures to be formed within the glass network. In addition, the peak barely moves during the entire experiment, showing that the poling environment has very little effect on the cathode side of the glass. In addition, the $Si\text{-}O^-$ peak stays at around 940 cm^{-1} throughout the poling experiment in both of the two

environments. The environment does not significantly affect the silicon oxygen structure on the cathode side of the glass.

The only major differences between the cathode side of the samples poled in the two different environments is that the Si-O-Si asymmetric vibrational peak seems to be more variable in the nitrogen environment. In this case, the slight inconsistency can be attributed to unidentified inconsistencies in the experimental procedure. In the future, these experiments should be repeated and a larger size of times of poling should be used.

Peaks between 2200 cm^{-1} and 4000 cm^{-1} include crucial information about the presence or the absence of molecular water and other hydrous species. However, as explained in the introduction and shown in Figures 4 and 5, SR-IR results from this region include part of the IR beam that has been reflected from both the surface of the glass and the backside[14]. These results do not give reliable information on the surface structure of the glass, rather they give information on both the anode and cathode side[14]. Figure 15 below shows the SR-IR spectra of samples poled in a humid environment. Both the anode side and the cathode side are shown and the spectra displayed goes from 4000-2200 cm^{-1}.

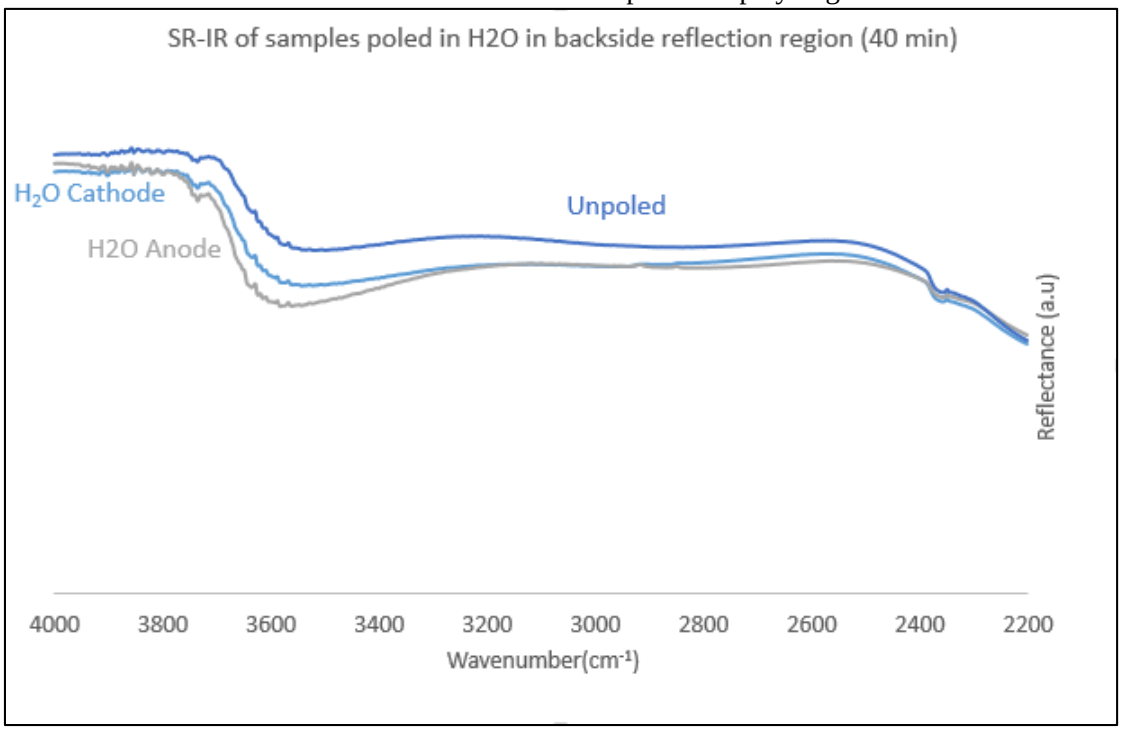

Figure 15: SR-IR spectra of sample poled in H2O environment taken on anode, cathode, and unpoled area of glass.

The key feature of the Figure 15 is that the anode and cathode spectra are virtually indistinguishable. They both exhibit negative peaks at approximately 3600 cm^{-1} and these peaks have similar intensities. The reason the two spectra are nearly identical is because backside reflection essentially adds the anode spectra to the cathode spectra when SR-IR of the cathode spectra is taken and the reverse happens when the SR-IR spectra of the anode is taken. Because of this issue, ATR-IR must be used to gain a reliable spectra of the surface of each sample above 2200 cm^{-1}.

ATR-IR Results

Because of backside reflection in SR-IR results for the spectrum above 2200 cm^{-1}, ATR-IR spectroscopy needs to be used to determine the changes at the surface of the glass in the region between 2200 cm^{-1} and 4000 cm^{-1}. This region can give accurate information on the presence or absence of water and hydrous species in the surface of the glass, which SR-IR could not provide reliable data on.

The ATR-IR data can show how water vapor in the atmosphere during poling effects the presence of hydrous species in the glass network at both the cathode and anode surface as a function of time. In the ATR spectra, a broad peak between 3650-2500 cm^{-1} indicates the presence of Si-OH and hydrous species, and a sharp peak around 1600 cm^{-1} indicates the presence of molecular water. Below, in figures 16 and 17, the ATR-IR spectra of samples poled in a humid environment are shown over different duration poling times. Figure 16 shows the anode side spectra and Figure 17 shows the cathode side spectra.

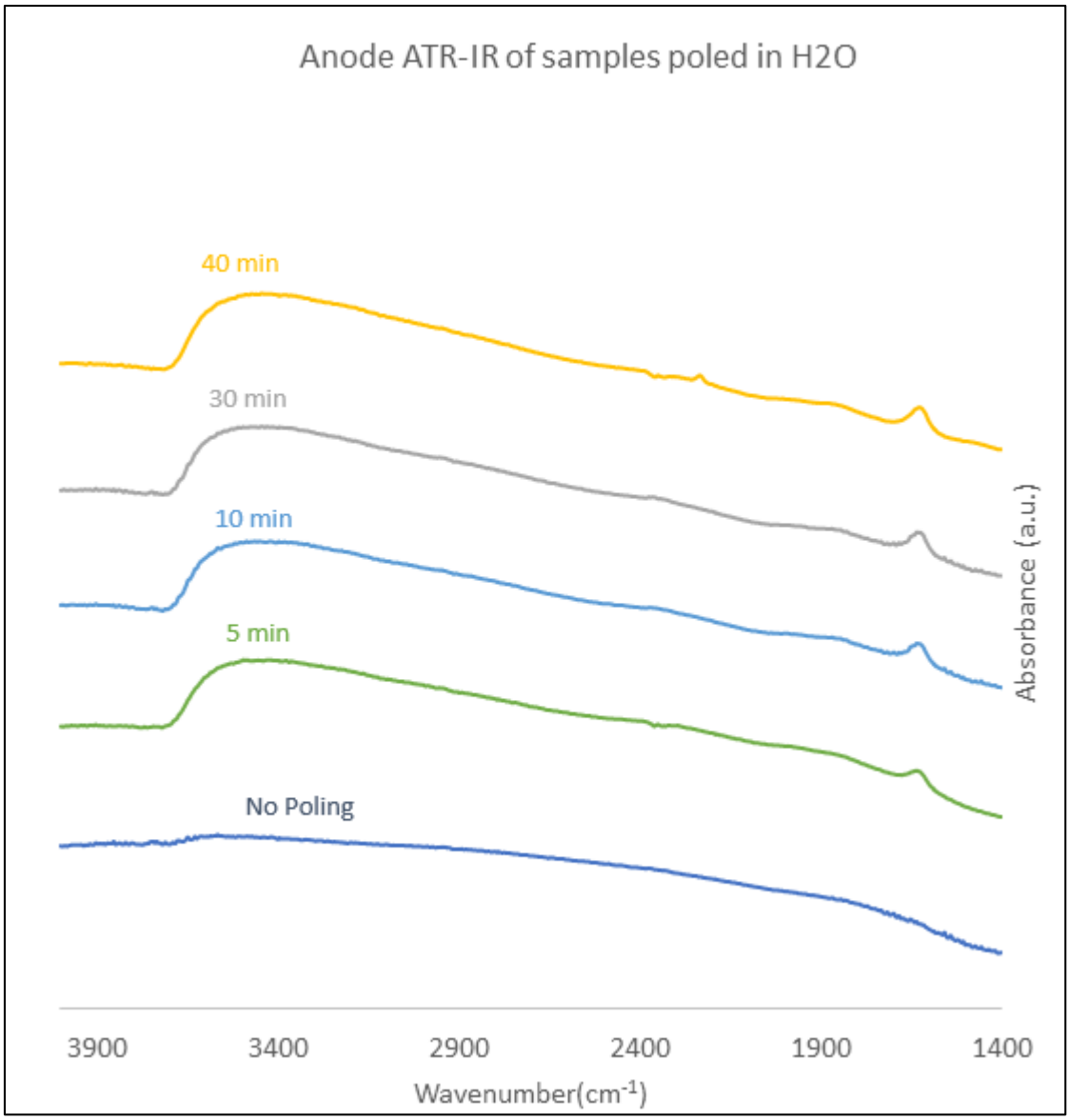

Figure 16: ATR-IR of anode side of glass samples poled for 0, 5, 10, 30 & 40 minutes. Data Credit: Jiawei Luo

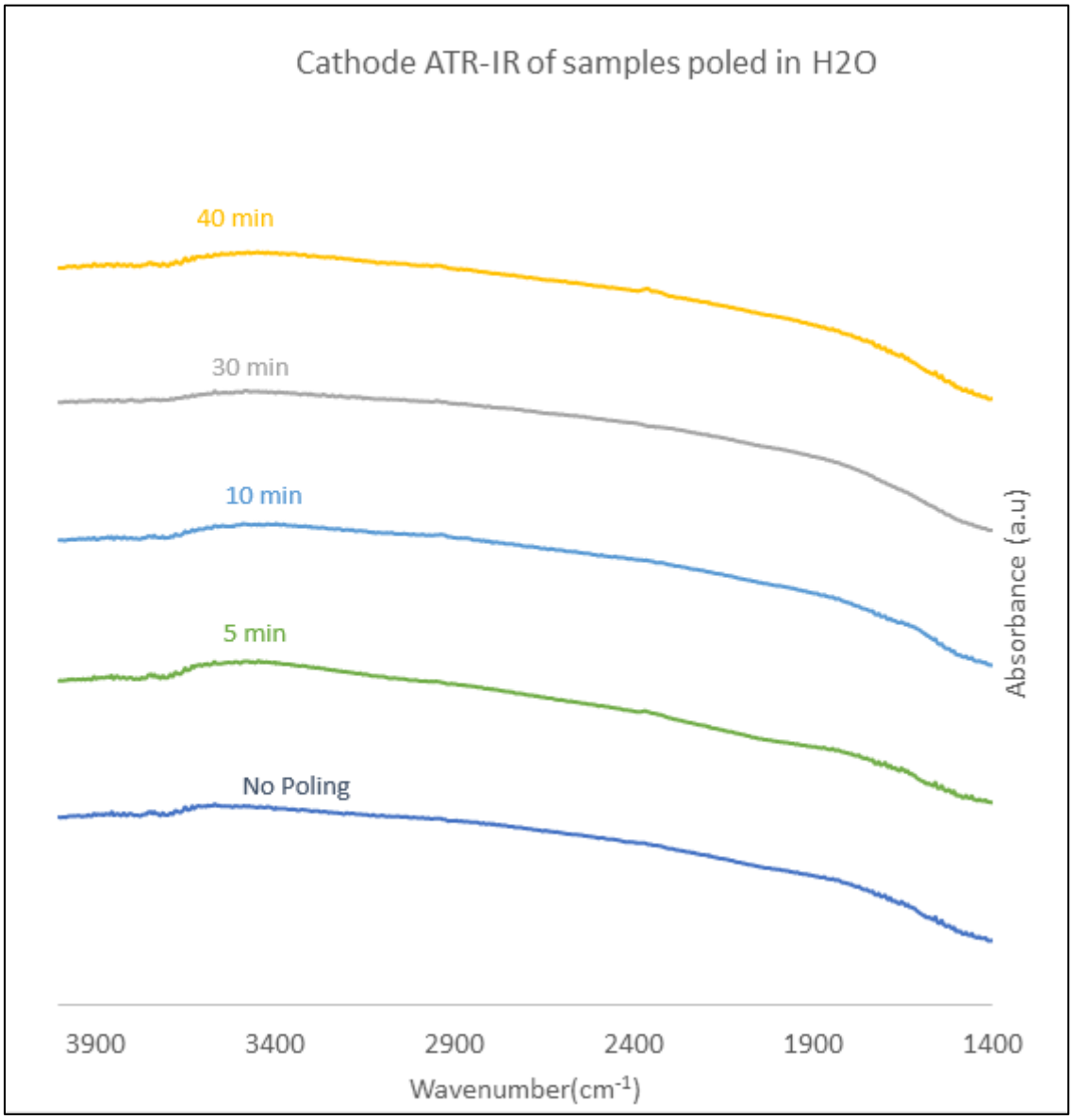

Figure 17: ATR-IR of cathode side of glass samples poled for 0, 5, 10, 30 & 40 minutes. Data Credit: Jiawei Luo

The ATR-IR results for both the cathode and anode side are somewhat expected. The anode side of the glass shows evidence of both Si-OH (broad 3650-2500 cm^{-1} peak) groups and molecular water (sharp peak at 1600 cm^{-1}) in all four poled samples. There is an essentially negligible Si-OH peak on the cathode side which is also seen on the un-poled glass, so only a small amount of water was absorbed into the glass structure on the cathode side. This makes sense because sodium moved into this region, essentially taking all of the locations where water could possibly be absorbed. The Si-OH stretching peak suggests some

hydrous species could have been introduced into the cathode side, but based on the SR-IR results this introduction is not significant enough to effect the silicon oxygen structures. There is also no sharp peak for molecular water on the cathode side.

One surprising feature of the ATR-IR spectrum is that the intensity of the Si-OH peak does not seem to change with poling time. Even after five minutes the peak is just about as large as after 40 minutes. The molecular water peak does increase slightly between five and forty minutes. During previous studies, when glass samples are poled in air, there is a significant increase in the amount of water and hydroxyl groups as poling time increases[10]. In ambient conditions, the amount of water in the environment is low compared with the humid environment. This trend seems to suggest that water quickly moves into the glass structure in the submicron layer because there is a greater driving force from the concentration gradient when samples are poled in a humid environment versus when samples are poled in air. This result alone cannot provide proper explanation for the gradual changes of the Si-O-Si network. One possible explanation for this phenomenon is that while water and hydrous species temporarily stabilize non-bridging oxygen groups ($Si\text{-}O^-$), the higher thermodynamic stability of the bridging structure slowly wins out and continues to form more Si-O-Si bridging groups. This hypothesis is not confirmed by these results, however, future experiments could help to clarify this phenomenon. By using different ATR crystals, like diamond which has a penetration depth about 3 times the distance of the germanium crystal, we can investigate how long and exactly where water molecules are located as poling goes on. Regardless, the evidence suggests that water and hydrous species are absorbed into the anode side of the glass and appear in the ATR-IR spectra when the sample is poled in a humid environment.

In order to confirm that water is being absorbed onto the surface and transferred to the subsurface region of the glass structure *during poling*, some samples were poled in deuterated water environments and ATR-IR spectra of these samples were collected to confirm that D_2O could be detected in the subsurface region of the glass just as H_2O was detected.

Samples poled for varying times in a deuterated water environment were investigated using ATR-IR and the results are shown below in Figure 18.

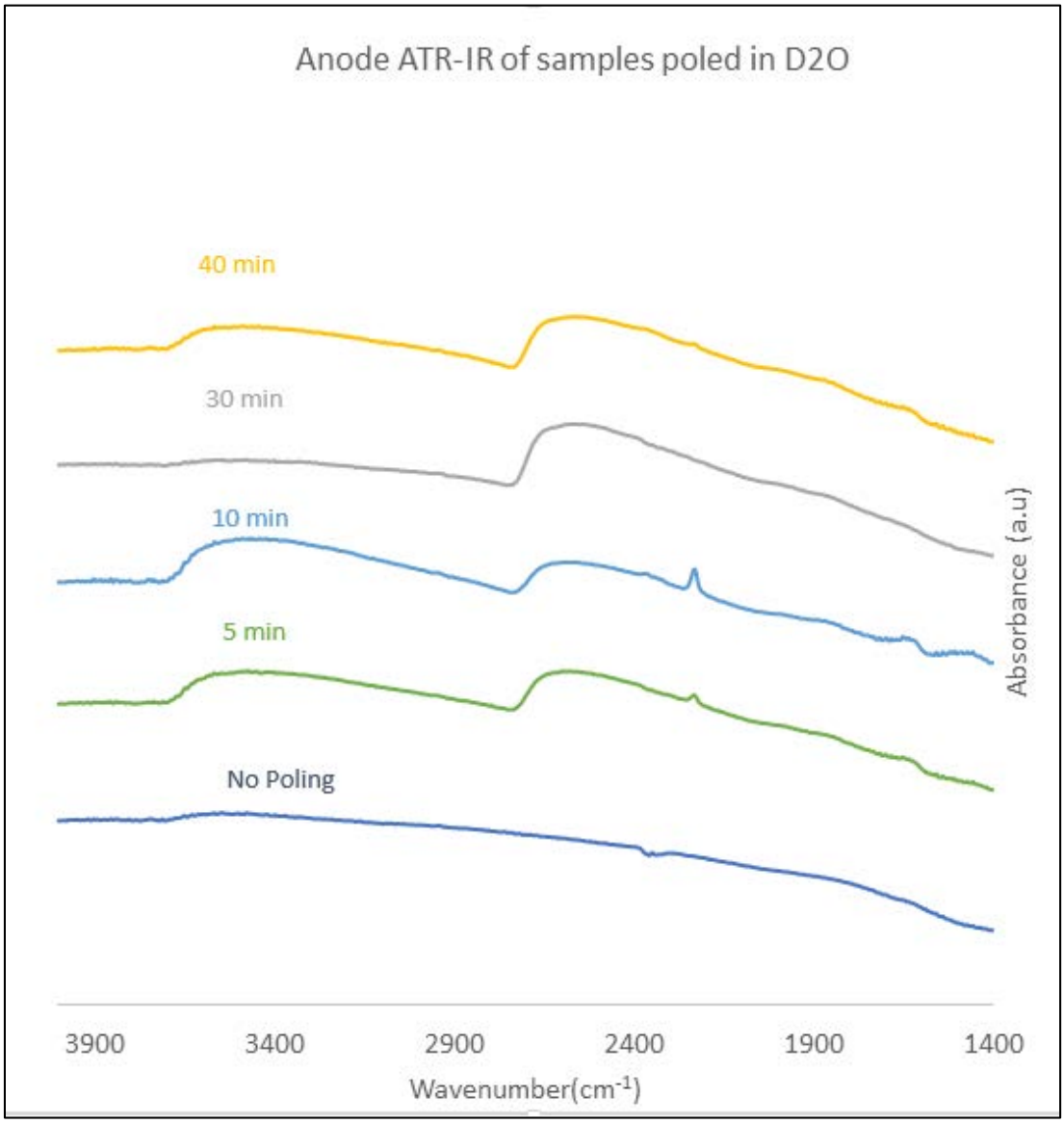

Figure 18: ATR-IR spectra on anode side of samples poled in D2O environment for 0, 5, 10, 30, and 40 minutes. Data Credit: Jiawei Luo.

As mentioned previously, Si-OD groups in ATR-IR have the same broad peak characteristic of Si-OH groups, but it is red-shifted significantly. The general relationship between OH and OD vibrational frequency is inversely proportional to the square root of the ratio of the reduced masses of OH and as shown below in Equation 4.

$$\Big/\sqrt{\frac{\frac{MW_O MW_H}{MW_O+MW_H}}{\frac{MW_O MW_D}{MW_O+MW_D}}} = \frac{\nu(O-H)}{\nu(O-D)} = 1.375 \quad (4)$$

By multiplying the broad OD peaks from 2700 cm^{-1} to 2200 cm^{-1} by the factor of 1.375, the peak shape and position shifts to look similar to the OH peak seen in previous Figures 15 and 16. The same is true for the presence of molecular water and molecular D_2O in the glass. Interestingly, the spectra for the D_2O samples still show the broad Si-OH peak at a lower intensity. This could be due to limited experimental control in that stored D_2O slowly will convert back to H_2O, and so some of the D_2O vapor introduced into the poling environment inevitably was H_2O. The broad, D_2O peak for all four poled samples (starting at around 2800 cm^{-1}) shows that the water found in both the SR-IR and ATR-IR spectra did, in fact, come from the poling environment and not from one of the washing steps. One more important fact about the D_2O spectra is that the molecular water peak is barely present and in the case of the 10 minute sample there are two small peaks, one at 1600 cm^{-1} and one at approximately 1450 cm^{-1}. These two peaks represent molecular water and molecular D_2O respectively. Again, the molecular water peak observed in previous IR results does in fact come in during poling, which is evidence for the movement of full molecules of water into the anode side of the glass during poling. Because molecular water is uncharged, it almost certainly plays the role of stabilizing Si-O- groups once sodium ions leave.

The ATR-IR spectra of samples poled in the nitrogen environment are shown below in Figure 19.

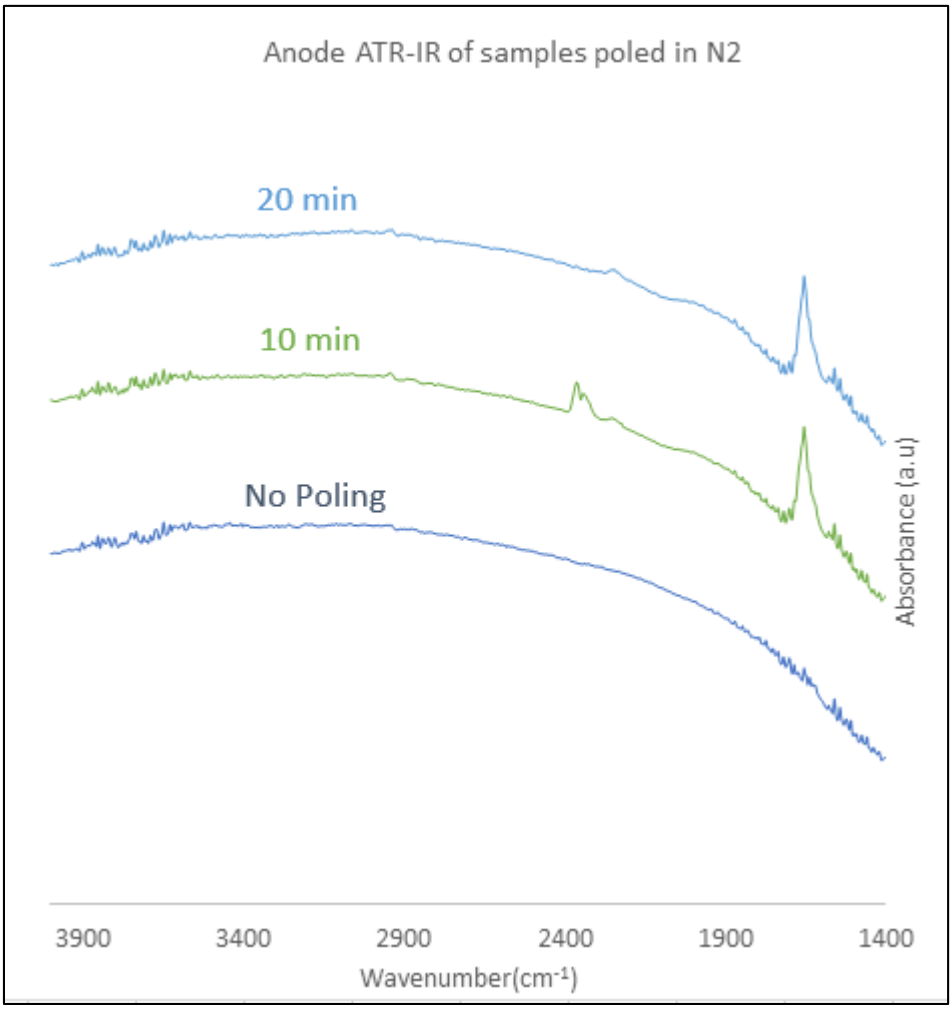

Figure 19: ATR-IR spectra of samples poled in nitrogen environment for 0, 10, and 20 minutes on anode side. Data Credit: Jiawei Luo.

Figure 19 shows the spectrum on the anode side of the glass after no poling, 10 minutes of poling and 20 minutes of poling. The most striking feature of the spectra is that between 3650-2500 cm^{-1} there is no evidence of a Si-OH peak that is seen in Figure 15. Going from a pristine sample to poling for 20 minutes the nitrogen does not introduce any hydrous species into the glass network. A peak does develop at around 1650 cm^{-1} which is typically associated with molecular water. However, in this case, because of the absence of a significant amount of molecular water, the peak can be attributed to the stretching vibration of nitric oxide present in the glass structure. The stretching vibration for nitric oxide has been found to occur between 1590-1650 cm^{-1} [29]. The source of this peak must still be confirmed in future work. If samples are poled in an Argon environment, similar spectra should be obtained, except the nitric oxide

peak should not appear, if that truly is the source of the peak at 1650 cm^{-1}. The ATR-IR of the cathode side of the nitrogen poled samples is shown in Figure 20.

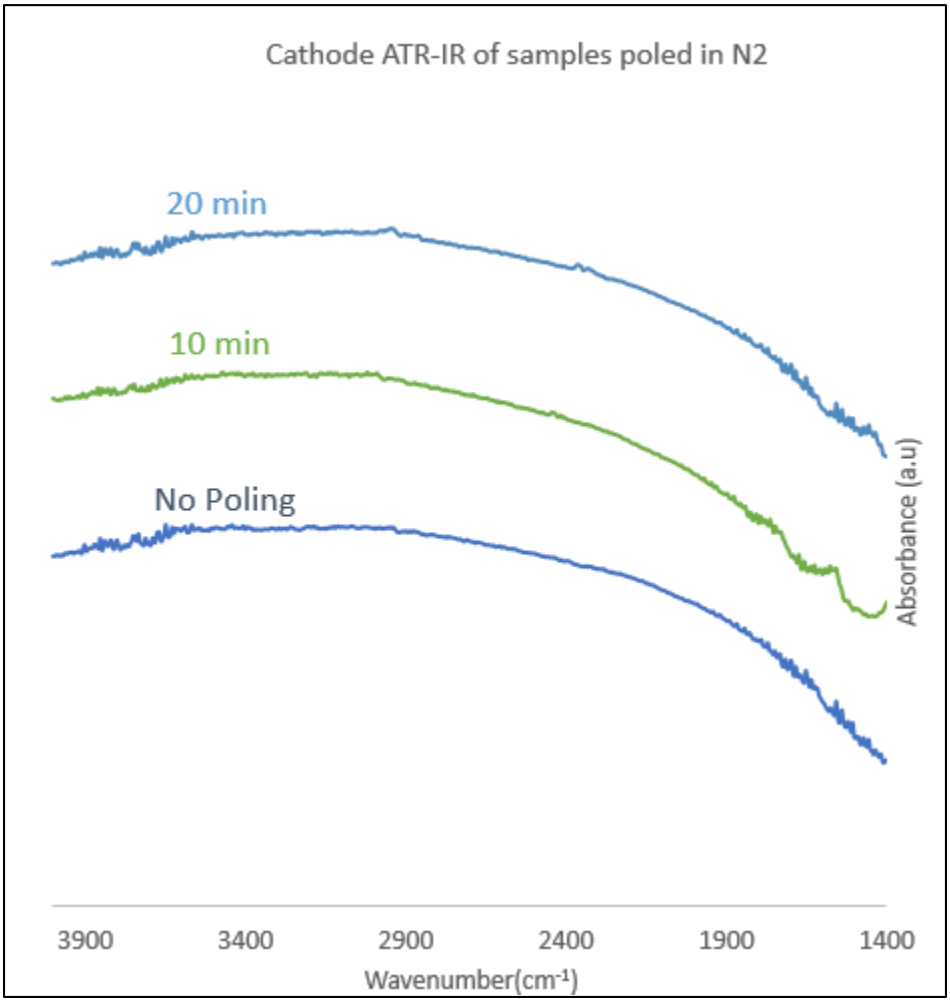

Figure 20: ATR-IR spectra of samples poled in nitrogen environment for 0, 10, and 20 minutes on cathode side. Data Credit: Jiawei Luo

Figure 20 is almost identical to Figure 18, except for the fact that the cathode side does not have the peaks at 1650 cm^{-1} indicative of nitric oxide. The absence of these peaks on the cathode side suggests that the nitric oxide groups play some role or are a result of the charge movement in the subanodic region. By comparing these ATR-IR spectra of samples poled in nitrogen to the ATR-IR spectra of the samples poled in humid environments, it is clear that the environment directly influences the structure of the glass at the surface.

The ATR-IR and SR-IR results suggest that the environment does significantly affect the mechanism of thermal poling and the resulting structure of the subanodic surface of the glass. SR-IR suggests that, in humid environments, water and other hydrous species play a role in stabilizing vacated NBO structures as some of the NBO groups transition to BO groups. While, in a nitrogen environment, that stabilization effect does not occur and the NBO groups primarily and quickly switch to BO groups during poling. ATR-IR confirms that during poling, molecular water and hydrous species are absorbed into the surface subanodic region when poled in humid conditions.

Chapter 4

Conclusions and Future Work

SR-IR and ATR-IR analysis were used to analyze the results of soda-lime glasses poled in H_2O, D_2O, and N_2 rich environments. All samples were poled at 200° C at 2kV and H_2O and D_2O vapors were introduced by bubbling air through liquid water and D_2O in a silicon bead packed tube. The SR-IR results were useful for determining the change in the Si-O-Si structure at the surface of the glass while ATR-IR was needed to investigate the presence of water and hydrous species at the surface of the glass after poling. SR-IR and ATR-IR analyses confirm the fact that thermal poling environment, particularly the presence or absence of water vapor, significantly affects the surface structure of soda-lime glass during thermal poling. In addition, the IR results suggest that based on the environment, the mechanism of the chemical rearrangement of the glass structure at the anode surface of the glass is effected by the environment.

One possible explanation for the results is that, in samples poled in a nitrogen environment, the sodium moves quickly through the glass structure, but then, because of a lack of secondary mechanisms, the structure stops rearranging quickly and current drops off. When poling in nitrogen, vacated $Si\text{-}O^-$ groups convert quickly to Si-O-Si because of a lack of stabilizing hydrous species. When poling in humid environments, water is able to stabilize intermediate $Si\text{-}O^-$ structures by creating Si-OH groups which require a lower activation energy to form than Si-O-Si groups. These Si-OH groups slow down the formation of Si-O-Si groups in the network, but $Si\text{-}O^-$ and Si-OH groups continue to convert to Si-O-Si over time. This stabilization mitigates charge in the subanodic region, but because the subanodic structure continues to rearrange for some time, charge continues to move through the glass for some time. This explanation of the poling results agrees mostly with Dussauze et al. and Lepienski et al.

In order to gain more solid evidence for the explanation above, more characterization of the surface during poling needs to be conducted. XPS could be used to gather data confirming what kind of functional groups exist at the surface of the soda-lime glass after poling in each type of environment.

Mechanical strength tests need to be conducted to see what the exact effect of the structural changes discussed in this thesis have on mechanical properties of the glass. In addition, poling in different relative humidities and analyzing Si-O-Si structure in the resulting glasses, coupled with mechanical strength tests would help to determine the optimal conditions for forming the strongest surface structure of the glass.

Forming stronger glass surfaces using thermal poling has applications in the glass manufacture industry and could help to save money by replacing expensive glasses like quartz with cheap, thermally poled soda-lime glasses. Thermally poled glasses could act as replacements for traditional glass coatings and thus protect the surface of glasses and enhance it without the addition of more chemicals. If thermal poling is to be used in any industrial application for the modification and strengthening of glass, optimal environmental conditions and an understanding of the chemical changes resulting from this thermal poling need to be understood. This thesis contributes to the overall understanding of the thermal poling process and the effect of environmental conditions on structure; future work needs to address the effect of the environment on mechanical properties.

Appendix

List of Experiments and Samples

Table 2: List of Experimental Conditions

Experiment #	Date Poled	Conditions	Location	Sample	Set tempe	Time (min)	Voltage (kV)	Cathode
1	9/4/2014	Air	Lab Drawer	Asahi 700 µm	200	20	2	HOPG
2	9/11/2014	Air	Lab Drawer	Asahi 700 µm	200	40	2	HOPG
3	9/22/2014	Air	Unknown	Asahi 700 µm	200	5	2	HOPG
4	9/22/2014	Air	Unknown	Asahi 700 µm	200	15	2	HOPG
5	9/25/2014	Air	Unknown	Asahi 700 µm	200	10	2	HOPG
6	9/25/2014	Air	Unknown	Asahi 700 µm	200	5	2	HOPG
7	10/2/2014	Air	Unknown	Asahi 700 µm	200	5	2	HOPG
8	10/2/2014	Air	Unknown	Asahi 700 µm	200	40	2	HOPG
9	10/16/2014	Air	Lab Drawer	Asahi 700 µm	200	90	2	HOPG
10	1/27/2015	Air	D2O/H20 Box	Asahi 700 µm	200	40	2	HOPG
11	2/3/2015	Air	D2O/H20 Box	Asahi 700 µm	200	40	2	HOPG
12	2/10/2015	Air	D2O/H20 Box	Asahi 700 µm	200	40	2	HOPG
13	2/17/2015	Air	D2O/H20 Box	Asahi 700 µm	200	20	2	HOPG
14	2/17/2015	Air	D2O/H20 Box	Asahi 700 µm	200	40	2	HOPG
15		Air	Jiawei/Corning?	Asahi 700 µm	200	40	2	SS
16		Air	Jiawei/Corning?	Asahi 700 µm	200	20	2	SS
17	2/26/2015	Air	Erik Poling 1	Asahi 700 µm	200	10	2	SS
18		Air	Jiawei/Corning?	Asahi 700 µm	200	40	2	SS
19		Air	Jiawei/Corning?	Asahi 700 µm	200	20	2	HOPG
20	3/17/2015	Air	Jiawei/Corning?	Asahi 700 µm	200	40	2	HOPG
21	3/31/2015	Air	Erik Poling 2	Asahi 700 µm	200	5	2	SS
22	3/31/2015	Air	Erik Poling 2	Asahi 700 µm	200	10	2	SS
23	4/14/2015	Air	Left Out for Jiawe	Asahi 700 µm	200	5	2	SS
24	4/28/2015	Air		Asahi 700 µm	200	10	2	SS
25	4/30/2015	Air		Asahi 700 µm	200	70	2	SS
2.1	10/2/2014	Air	D20/H20 Box	Asahi 700 µm	250	10	2	HOPG
2.2	10/2/2014	Air	Unknown	Asahi 700 µm	250	20	2	HOPG
3.1	10/6/2014	Air	Lab Drawer	Asahi 700 µm	300	10	2	HOPG
4.1	10/22/2014	Air	Lab Drawer	Asahi 700 µm	200	20	2	HOPG
4.2	10/22/2014	Air	Lab Drawer	Asahi 700 µm	200	40	2	HOPG
4.3	10/30/2014	Air	Lab Drawer	Asahi 700 µm	200	30	2	HOPG
4.4	10/31/2014	Air	Lab Drawer	Asahi 700 µm	200	30	2	HOPG
5.1		D2O Flow		Asahi 700 µm	200	30	2	HOPG
5.2	11/4/2014	D2O Flow	Erik Poling 2	Asahi 700 µm	200	20	2	HOPG

5.3	11/12/2014	D2O Flow	Erik Poling 2	Asahi 700 µm	200	10	2	HOPG
5.4	12/11/2014	D2O Flow	Erik Poling 1	Asahi 700 µm	200	5	2	HOPG
5.5	1/13/2015	D2O Flow	Erik Poling 1	Asahi 700 µm	200	20	2	HOPG
5.6	1/13/2015	D2O Flow	Erik Poling 2	Asahi 700 µm	200	15	2	HOPG
5.7	1/13/2015	D2O Flow	Erik Poling 1	Asahi 700 µm	200	30	2	HOPG
5.8		D2O Flow	Jiawei	Asahi 700 µm	200	40	2	HOPG
5.9	2/25/2015	D2O Flow	Erik Poling 1	Asahi 700 µm	200	40	2	SS
5.10	3/24/2015	D2O Flow	Jiawei	Asahi 700 µm	200	40	2	SS
5.11	3/24/2015	D2O Flow	Jiawei	Asahi 700 µm	200	10	2	SS
5.12	4/21/2015	D2O Flow	Erik Poling Big Co	Asahi 700 µm	200	5	2	SS
5.13	4/21/2015	D2O Flow	Erik Poling Big Co	Asahi 700 µm	200	10	2	SS
5.14	4/21/2015	D2O Flow	Erik Poling Big Co	Asahi 700 µm	200	20	2	SS
5.15	4/28/2015	D2O Flow		Asahi 700 µm	200	10	2	SS
6.1		H2O Flow	Jiawei	Asahi 700 µm	200	10	2	HOPG
6.2	11/12/2014	H2O Flow	Erik Poling 2	Asahi 700 µm	200	20	2	HOPG
6.3	11/20/2014	H2O Flow	Erik Poling 1	Asahi 700 µm	200	20	2	HOPG
6.4	11/20/2014	H2O Flow	Erik Poling 1	Asahi 700 µm	200	40	2	HOPG
6.5		H2O Flow	Erik Poling 2	Asahi 700 µm	200	10	2	HOPG
6.6	12/18/2014	H2O Flow	Jiawei	Asahi 700 µm	200	5	2	HOPG
6.7	1/15/2015	H2O Flow	Erik Poling 1	Asahi 700 µm	200	30	2	HOPG
6.8		H2O Flow	Jiawei	Asahi 700 µm	200	40	2	HOPG
6.9	4/7/2015	H2O Flow	Erik Poling 2	Asahi 700 µm	200	10	2	SS
6.10	4/14/2015	H2O Flow	Left Out for Jiawe	Asahi 700 µm	200	5	2	SS
6.11	4/28/2015	H2O Flow		Asahi 700 µm	200	10	2	SS
6.12	4/30/2015	H2O Flow		Asahi 700 µm	200	40	2	SS
7.1	3/31/2015	N2 Flow	Erik Poling 2	Asahi 700 µm	200	20	2	SS
7.2	4/2/2015	N2 Flow	Erik Poling 2	Asahi 700 µm	200	40	2	SS
7.3	4/2/2015	N2 Flow	Erik Poling 2	Asahi 700 µm	200	10	2	SS
7.4	4/7/2015	N2 Flow	Erik Poling 2	Asahi 700 µm	200	20	2	SS
7.5	4/7/2015	N2 Flow	Jiawei	Asahi 700 µm	200	5	2	SS
7.6	4/14/2015	N2 Flow	Left Out for Jiawe	Asahi 700 µm	200	5	2	SS
7.7	4/16/2015	N2 Flow	Erik Poling Big Co	Asahi 700 µm	200	20	2	SS

REFERENCES

1. Congcal Calcium Carbonate. Glass. http://www.congcal.com/markets/glass (accessed March 28, 2015).
2. Varshneya, A. K. *Fundamentals of Inorganic Glasses,* 1st ed.; Academic Press: San Diego, 1994.
3. Pantano, C.G. Surface Chemistry in Relation to the Strength and Fracture of Silicate Glasses. In *Strength of Inorganic Glass;* Kurkjian C. R., Ed.; Plenum: New York, 1985; pp 37–66.
4. Carlson, D.E.; Hang, K.W.; Stockdale, G.F.; Electrode "Polarization" in Alkali-Containing Glasses. *J. Am. Ceram. Soc.* **1972**, *55*, 337-341.
5. Dussauze, M.; Rodriguez, V.; Lipovskii, A.; Petrov, M.; Smith, C.; Richardson, K.; Cardinal, T.; Fargin, E.; Kamitos, E.I.; How Does Thermal Poling Affect the Structure of Soda-Lime Glass? *J. Phys. Chem.* **2010,** *114*, 12754–12759.
6. Österberg, U.; Margulis, W.; Dye laser pumped by Nd:YAG laser pulses frequency doubled in a glass optical fiber. *Opt. Lett.* **1986,** *11,* 516-518.
7. Chemistry of Glass. Pilkington. https://www.pilkington.com/pilkington information/about+pilkington/education/chemistry+of+glass.htm (accessed Oct. 28, 2015)
8. Kreiger, U.K.; Lanford, W.A; Field assisted transport of Na^+ ions, Ca^{2+} ions and electrons in commercial soda-lime glass I: experimental. *J. Non-Cryst. Solids. Chem.* **1988,** *102*, 50-61.
9. He, H.; Qian, L.; Pantano, C.G.; Kim, S.H.; Mechanochemical wear of soda lime silica glass in humid environments. *J. Am. Ceram. Soc.* **2014**, *97,* 2061-2068.
10. Luo, J.; He, H.; Podraza, N.J.; Qian, L.; Pantano, C.J.; Kim, S.H.; Thermal poling of soda lime silica glass with nonblocking electrodes – Part 1: Effects of sodium ion migration and water ingress on glass surface structure. *In Progress.*
11. He, H.; Luo, J.; Qian, L.; Pantano, C.J.; Kim, S.H.; Thermal poling of soda lime silica glass with non-blocking electrodes – Part 2: Effects on mechanical and mechanochemical properties. *In Progress.*
12. Bradley, L.C.; Dilworth, Z.R.; Barnette, A.L.; Hsiao, E.; Barthel, A.J.; Pantano, C.J.; Kim, S.H.; Hydronium ions ions in soda-lime silicate glass surfaces. *J. Am. Ceram. Soc.* **2013**, *96*, 458-463.
13. Alley, T.G.; Brueck, S.R.J.; Myers, R.A.; Space charge dynamics in thermally poled fused silica. *J. Non-Cryst. Solids.* **1998**, *242*, 165-176.
14. Amma, S.; Luo, J.; Pantano, C.G.; Kim, S.H.; Specular reflectance (SR) and attenuated total reflectance (ATR) infrared (IR) spectroscopy of transparent flat glass surfaces: A case study for soda lime float glass. *J. Non-Cryst. Solids.* **2015**. Web.
15. Geotti-Bianchini, F.; De Rui, L.; Gagliardi, G.; Guglielmi, M.; Pantano, C.G.; New interpretation of the IR reflectance spectra of SiO2 rich films on soda lime glass. *Glastech. Ber.* **1991**, *64*, 205-217.

16. Geotti-Bianchini, M.; Preo, L.; Guglielmi, M.; Pantano, C.G.; Infrared reflectance spectra of semi-transparent SiO2 rich films on silicate glasses: influence of the substrate and film thickness. *J. Non-Cryst. Solids.* **2003**, *321*, 110-119.
17. Lowenstern, J.B.; Pitcher, B.W.; Analysis of H2O in Silicate Glass Using Attenuated Total Reflectance (ATR). Micro-FTIR Spectroscopy. *Am. Mineral.* **2013,** *98,* 1660-1668.
18. Compton, S.V.; Compton, D.A.C.; Optimization of data recorded by internal reflectance spectroscopy. In *Practical Sampling Techniques for Infrared Analysis;* Coleman, P.B., Ed.; CRC Press: Boca Raton, 1993: pg. 301.
19. Uchino, T.; Sakka, T.; Iwasaki, M.; Interpretation of hydrated states of sodium silicate glasses by infrared and raman analysis. *J. Am. Ceram. Soc.* **1991**, *74*, 306-313.
20. Uchino, T.; Sakka, T.; Hotta, K.; Iwasaki, M.; Attenuated total reflectance fourier transform infrared spectra of a hydrated sodium silicate glass. *J. Am. Ceram. Soc.* **1989**, *72*, 2173-2175.
21. Lepienski, C.M.; Giacometti, J.A; Ferreira, G.F.; Freire Jr., F.L.; Achete, C.A.; Electric Field distribution and near-surface modifications in soda-lime glass submitted to a dc potential. *J. Non-Cryst. Solids. Chem.* **1993,** *159*, 204-212.
22. Ziemath, E.C.; Araujo, V.D.; Escanhoela, C.A.; Compositional and structural changes at the anodic surface of thermally poled soda-lime float glass. *J. Appl. Phys.* **2008,** *104*. Web.
23. Carlson, D.E.; Anodic Proton Injection in Glasses. *J. Am. Ceram. Soc.* **1974**, *57*, 461-466.
24. Ernsberger, F.M.; The role of molecular water in the diffusive transport of protons in glasses. *Phys. Chem. Glasses* **1980,** *21*, 146-149.
25. Lanford, W.A.; Davis, K.; Lamarche, P.; Laursen, T.; Groleau, R.; Doremus, R.H.; Hydration of soda-lime glass. *J. Non-Cryst. Solids. Chem.* **1979,** *33*, 249-266.
26. Lepicard, A.; Cardinal, T.; Fargin, E.; Adamietz, F.; Rodriguez, V.; Richardson, K.; Dussauze, M.; Surface Reactivity Control of a Borosilicate Glass Using Thermal Poling. *J. Phys. Chem.* **2015,** *119*, 22999-23007.
27. Attenuated Total Reflection (ATR) – a versatile tool for FT-IR spectroscopy. Bruker Optics. https://www.bruker.com/fileadmin/user_upload/8-PDF-Docs/OpticalSpectrospcopy/FT-IR/ALPHA/AN/AN79_ATR-Basics_EN.pdf (accessed Nov. 9, 2015)
28. Launer, P.J.; Infrared Analysis of organosilicon compounds: spectra-structure correlations. Gelest. http://www.gelest.com/goods/pdf/Library/11Infra.pdf (accessed Nov. 18, 2015).
29. Magtoto, N. P.; Sefara, N.L.; Richardson, H.H.; Two dimensional FT-IR correlation analysis of the chemisorption of nitric oxide on Pt(100). *Appl. Spectrosc.* **1999**, *53*, 178-183.

ACADEMIC **VITA**

Erik Schneider
eschneider9611@gmail.com

Education

The Pennsylvania State University-B.S.in Chemical Engineering *(Graduate Dec. 2015)*
University of Auckland-School of Engineering Exchange *(Spring 2013)*

Work Experience

Process Development Intern, Mars Global Chocolate-*Hackettstown, NJ. (Summer 2015)*

- Wrote SOP and led project safety review for new surface treatment technology
- Designed experiments showing a possible 30% quality improvement and potential annual savings of $17,000

Engineering Co-op, Albemarle Corporation-*Tyrone, PA (Spring 2014)*

- Process engineering experience with specialty chemical company
- Communicated with process operators, building foremen, chemists, and other engineers to troubleshoot equipment issues, improve processes, and implement safety improvements
- Created 3-D model of Teflon nozzle sleeve to fix reactor and coordinated manufacture of the 3-D model by outside vendor-*Saved cost of relining 500 gallon reactor-$20,000*

Research and Development Intern, Avery-Dennison Corporation-*Mill Hall, PA. (Summer 2014)*

- Ran experiments and assisted with development of UV curing Design of Experiment (DOE) to optimize cost, performance, and footprint of future production equipment

Co-founder, DripRight drip irrigation systems-*University Park, PA (Fall 2013)*

- Founded drip irrigation company with small interdisciplinary team, selling affordable drip irrigation systems to rural farmers in Cameroon
- Made $1500 in sales in first 3 months of operation

Undergraduate Researcher, The Pennsylvania State University- *(Summer 2012-Fall 2015)*

- Investigated properties of potassium carbonate catalyst in industrial energy process
- Collected and analyzed spectroscopic data using ESEM, EDS, Boehm titration, and SR-IR techniques
- Investigated change in surface structure of glass during thermal poling process

Publications

"Physical and chemical changes of coal during catalytic fluidized bed gasification" *(Published Summer 2015)*

- Credited as second author in *Fuel Processing Technology* journal article

"The surface chemical and mechanical effects of thermal poling in different environments on soda-lime glass" *(In Progress)*

- Will be credited as second author

Activities

President, African Library Project *(Spring 2014-Spring 2015)*

- Managed supply-chain of collecting, packing, and shipping over 3,000 children's books to Africa
- Ran biweekly meetings, and delegated tasks to group of 5 officers

Phollegian Editor, Phroth Humor Publication *(Fall 2013-Spring 2015)*

- Wrote approx. 10 articles per publication for satirical newspaper, *The Phroth Phollegian*
- Responsible for final edits on monthly publication distributed to over 10,000 readers

Honors

Schreyer Honors Scholar *(2011-2015)*
Dean's List *(Fall 2011, Spring 2012, Fall 2012, Spring 2013, Fall 2013, Fall 2014, Spring 2015)*
College of Engineering Scholarship Recipient *(2011-2015)*